frontiers in Environmental Science

ORIGINAL RESEARCH
published: 15 October 2021
doi: 10.3389/fenvs.2021.642346

A Multi-Tracer Study of Fresh Water Sources for a Temperate Urbanized Coastal Bay (Southern Baltic Sea)

Cátia Milene Ehlert von Ahn[1], Jan C. Scholten[2], Christoph Malik[1,3], Peter Feldens[4], Bo Liu[5], Olaf Dellwig[1], Anna-Kathrina Jenner[1], Svenja Papenmeier[4], Iris Schmiedinger[1], Mary A. Zeller[1] and Michael Ernst Böttcher[1,6,7]**

[1]Geochemistry and Isotope Biogeochemistry Group, Leibniz Institute for Baltic Sea Research (IOW), Warnemünde, Germany, [2]Institute of Geosciences, Kiel University, Kiel, Germany, [3]Department of Hydrogeology, UmweltPlan GmbH Stralsund, Stralsund, Germany, [4]Marine Geophysics Group, Leibniz Institute for Baltic Sea Research (IOW), Warnemünde, Germany, [5]Section of Marine Geochemistry, Alfred Wegener Institute Helmholtz Centre for Polar and Marine Research, Bremerhaven, Germany, [6]Marine Geochemistry, University of Greifswald, Greifswald, Germany, [7]Maritime Systems, Interdisciplinary Faculty, University of Rostock, Rostock, Germany

OPEN ACCESS

Edited by:
Henry Bokuniewicz, The State University of New York (SUNY), United States

Reviewed by:
Aaron J. Beck, GEOMAR Helmholtz Center for Ocean Research Kiel, Germany
Olivier Radakovitch, Institut de Radioprotection et de Sûreté Nucléaire, France

***Correspondence:**
Cátia Milene Ehlert von Ahn
catia.vonahn@io-warnemuende.de
Michael Ernst Böttcher
michael.boettcher@io-warnemuende.de

Specialty section:
This article was submitted to Biogeochemical Dynamics, a section of the journal Frontiers in Environmental Science

Received: *15 December 2020*
Accepted: *03 September 2021*
Published: *15 October 2021*

Citation:
von Ahn CME, Scholten JC, Malik C, Feldens P, Liu B, Dellwig O, Jenner A-K Papenmeier S, Schmiedinger I, Zeller MA and Böttcher ME (2021) A Multi-Tracer Study of Fresh Water Sources for a Temperate Urbanized Coastal Bay (Southern Baltic Sea). Front. Environ. Sci. 9:642346. doi: 10.3389/fenvs.2021.642346

Terrestrial surface waters and submarine ground water discharge (SGD) act as a source of dissolved substances for coastal systems. Solute fluxes of SGD depend on the ground water composition and the water-solid-microbe interactions close to the sediment-water interface. Thus, this study aims to characterize and evaluate the hydrogeochemical gradients developing in the fresh-salt water mixing zone of the Wismar Bay (WB), southern Baltic Sea, Germany. Sampling campaigns covering the WB, the fresh-salt water mixing zone at the beach of the WB shoreline, terrestrial surface and ground waters near the WB as well sediments pore water were carried out. In these different waters, the distribution of dissolved inorganic carbon, nutrients, major ions, trace elements, stable isotopes (H, O, C, S), and radium isotopes have been investigated. Enhanced concentrations of radium isotopes together with dissolved manganese, barium in the surface waters of the eastern WB indicated benthic-pelagic coupling via the exchange between pore water and the water column. Salinity, stable isotopes, and major ions in sediment pore water profiles identified the presence of fresh ground water below about 40 cmbsf in the central part of the bay. Geophysical acoustic techniques revealed the local impact of anthropogenic sediment excavation, which reduced the thickness of a sediment layer between the coastal aquifer and the bottom water, causing, therefore, a ground water upward flow close to the top sediments. The fresh impacted pore water stable isotope composition ($\delta^{18}O$, $\delta^{2}H$) plot close to the regional meteoric water line indicating a relatively modern ground water source. The calculated organic matter mineralization rates and the dissolved inorganic carbon sediment-water fluxes were much higher at the fresh impacted site when compared to other unimpacted sediments. Therefore, this study reveals that different fresh water sources contribute to the water balance of WB including a SGD source.

Keywords: urbanized coastal bay, submarine ground water discharge, subterranean estuary, hydrogeochemistry, stable isotope, radium isotope, acoustic survey, Wismar Bay

INTRODUCTION

Coastal regions are great of interest because they receive water and elements from the continents. Water drains the watershed towards the sea through surface water flow like rivers, coastal lagoons, and streams. In addition, ground waters may act as a further transport route for land-derived dissolved matter via submarine ground water discharge (SGD) (e.g., Johannes, 1980; Church, 1996; Burnett et al., 2003, Burnett et al., 2006; Moore 2010; Jurasinski et al., 2018).

A combination of the enhanced material transport and high pelagic productivity in coastal regions lead to an intensive benthic biogeochemical element recycling (Jørgensen and Kasten, 2006) and steep pore water gradients of, e.g., dissolved carbon species, nutrients, and major and trace elements to surface waters. SGD has been found to contribute to the overall oceanic water and element budget (e.g., Burnett et al., 2003; Santos et al., 2012), however, processes impacting the flux and associated solutes along the land-ocean continuum are considered as one of the unsolved problems in hydrology (Blöschl et al., 2019).

In contrast to rivers, where water discharge and their compositional variations are known in sufficient resolution and precision, the quantification of SGD entering coastal waters remains a challenge (e.g., Stieglitz et al., 2008; Rodellas et al., 2012; Douglas et al., 2020; Moosdorf et al., 2021). Therefore, more studies are needed combining different techniques to understand the dynamics in SGD and its role for water and element transfer on different scales (Burnett et al., 2006; Taniguchi, et al., 2019; Moosdorf et al., 2021; Rocha et al., 2021).

Common approaches to calculate SGD fluxes often rely on measurements of dissolved constituents in riverine and nearshore fresh ground water as endmembers, and assume conservative behavior of dissolved constituents across the mixing zone (Oberdorfer et al., 1990; Burnett et al., 2008; Rodellas et al., 2015; de Souza et al., 2021). However, due to the complexity of coastal aquifer mixing zones between ground water and sea water, it is a challenge to characterize the actual composition of solutions that finally discharge to the marine bottom waters (Cerdà-Domènech et al., 2017; Bejannin et al., 2020). This challenge is fostered by biogeochemical and associated physicochemical processes (e.g., mineralization of organic matter, ionic ad/desorption, mineral dissolution/precipitation) between fresh and saline pore water within the aquifer mixing zone that may lead to substantial changes in the composition of SGD-born element fluxes (e.g., Beck et al., 2007; Donis et al., 2017). These mostly redox-dependent processes in the subterranean estuary are more pronounced than those taking place in the oxic mixing zone of surface water estuaries (e.g., Moosdorf et al., 2021).

In many coastal areas, anthropogenic interventions may impact flow conditions and water balance (Stieglitz et al., 2007; Stegmann et al., 2011). For instance, dredging of canals in coastal areas may reduce the sediment cover on top of unconfined aquifers, thereby, enhancing the discharge of SGD and associated substances (Santos et al., 2008; Macklin et al., 2014; Teatini et al., 2017), or may promote salt water intrusions into aquifers (Moore, 1996). Moreover, an enhancement of coastal ground water exchange, e.g., caused by anthropogenic activities, may lead to an indirect enhancement of dissolved nutrient and carbon loads reflecting in changes in the biogeochemistry of surface waters (Lee et al., 2009).

Coastal areas of the southern Baltic Sea (BS) offer great opportunities to investigate the role of different fresh water inputs. Besides surface water inflows, SGD has been observed, for instance, in the Eckernförde Bay in the south-western BS (Whiticar and Werner, 1981; Schlüter et al., 2004). Other studies are focusing on the Puck Bay, in the southern BS (Jankowska et al., 1994; Szymczycha et al., 2012, 2020; Kotwicki et al., 2014; Donis et al., 2017; Böttcher et al., 2021) where significant discharge has been observed. The hydrogeology in these areas differs from those in the northwestern part of the BS, where multiple submarine fresh water sources were described that are only under minor impact by human activities (Krall et al., 2017; Virtasalo et al., 2019).

In the present study, investigations were conducted in the urbanized Wismar Bay (WB), southern BS (**Figure 1**). During a first survey carried out in 2012 along parts of the southern BS coastline comparably higher ^{224}Radium (^{224}Ra) activities were observed in surface waters of the WB (**Figure 2**). This suggested an enhancement of benthic-pelagic coupling, likely driven by SGD, which would agree with a tentative water balance for the WB (Schafmeister and Darsow, 2004). Moreover, the semi-enclosed WB is an interesting site to investigate inputs of water and substances, since the bay is under multiple anthropogenic impacts including port activities (VSW, 2018), making it similar to other modern coastal areas.

We combined a multi-isotope hydrochemical approach including a geophysical characterization of sedimentary structures to improve our understanding of fresh water sources into the WB. In addition, the biogeochemical processes taking place in the top sediments were modeled and investigated to understand the impact of SGD on their release of elements. The results show that different fresh water sources exist for the WB. SGD takes place at different areas through the bay, e.g., near the coastline, and in the central part of the bay. Anthropogenic activities, such as the creation of a navigation channel may cause a connection to unconfined aquifers and, therefore, promoting the exchange of water and associated elements with the WB bottom water.

METHODS

Study Area

The north-eastern part of Germany is characterized by a generally flat topography consisting of unconsolidated glacial sediments, humid climate conditions, urbanized cities, and often agricultural land use in the catchment basin. The present study was carried out in the WB (**Figure 1**), which is a coastal embayment in the southern BS, separated from the open BS by two shallow banks (Prena, 1995). Sediments in the bay are composed of quaternary glaciofluvial sands and intercalated tills (Schafmeister and Darsow, 2004). Maximum water depths of 10 m are in the western part of WB where muddy sediments are found, with

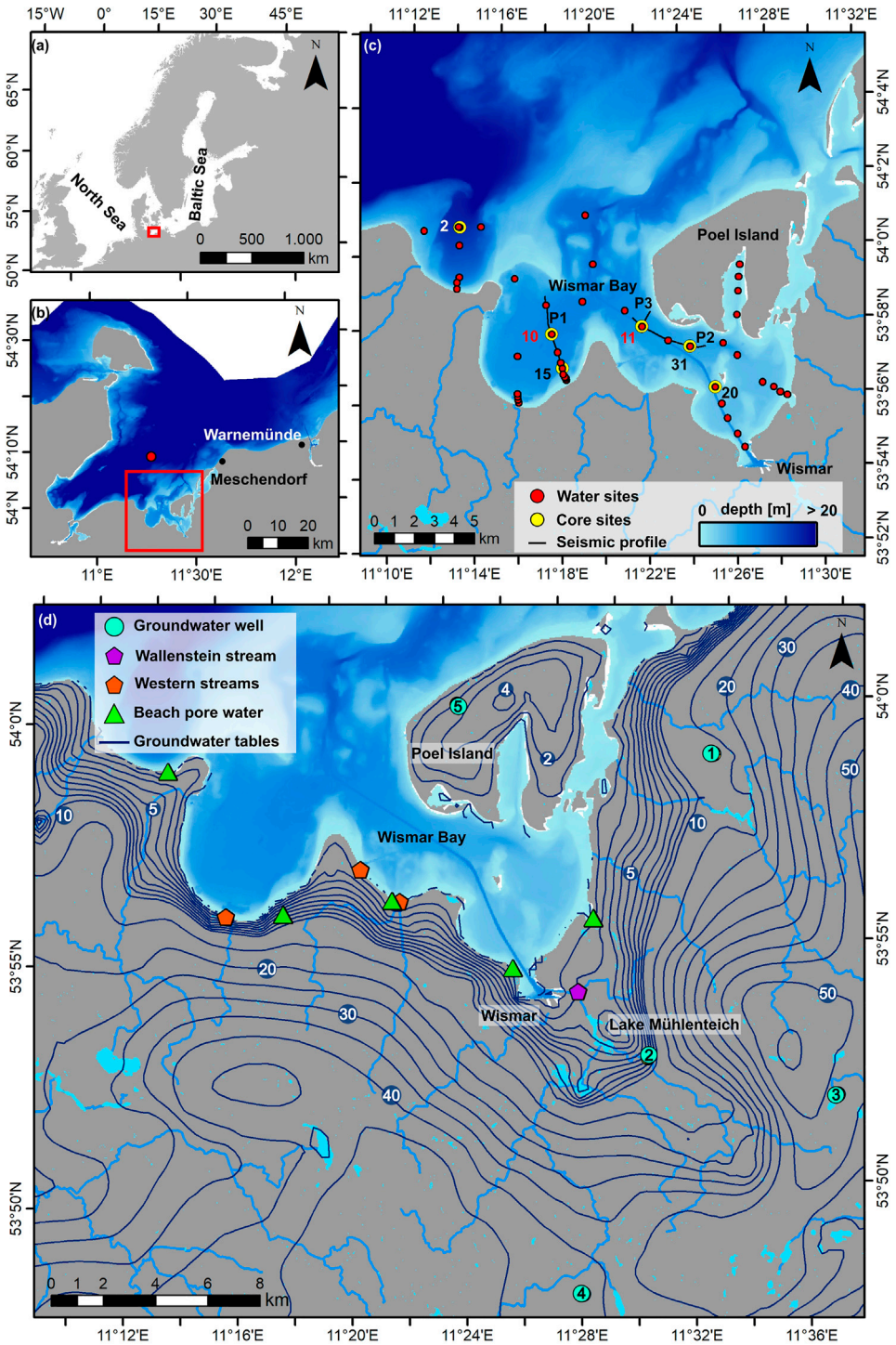

FIGURE 1 | Map of Baltic Sea and North Sea showing the location of the Wismar Bay **(A)**. Southern Baltic Sea, Germany shoreline showing the location of the Wismar Bay, including the adjacent investigated areas: Meschendorf, Warnemünde and, the surface water site at open Baltic Sea waters (red dot). Map of Wismar Bay with the sampling sites: surface water (red dots), sediment cores (yellow dots), the tracks of the seismic profiles (black line). The sediment cores are labeled, and the red numbers are the locations where SGD was found. **(C)**. Map of Wismar Bay and surrounding showing the ground water table (m), the streams discharging into the bay, and the lakes, as well as the ground water wells (cyan circles) also labeled, the sites at the western streams (orange diamond), Wallenstein stream (purple diamond), and the beach pore water sites (green triangle). The bathymetry highlighted the location of the navigation channel in the Wismar Bay. SOURCE: BSH, LUNG.

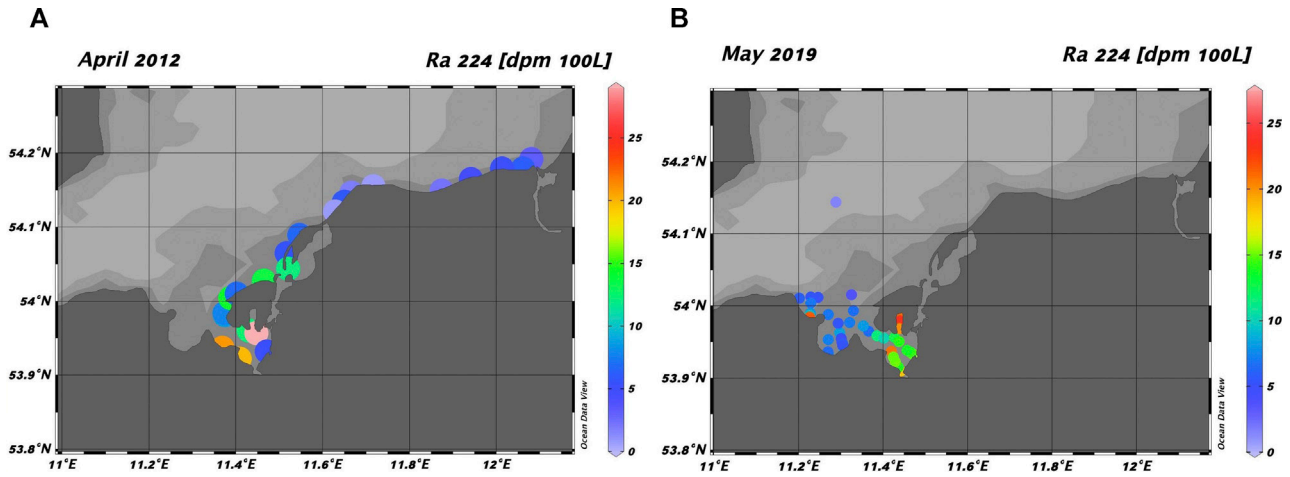

FIGURE 2 | Map of Germany coastline from WB to Warnemünde showing the activities of $^{224}Ra_{ex}$ in surface water from WB until Warnemünde carried out on April 2012 **(A)** and $^{224}Ra_{ex}$ in WB from the present study **(B)**.

sedimentary organic matter of up to 10% (Prena, 1995). Sandy sediments occur in the shallower areas.

The port of the town of Wismar is located on the east side of the bay, and ship navigation to the open BS is via an about 27 km long channel (**Figure 1**) (VSW, 2018).

The surrounding area of WB has three, each approximately 10 m thick aquifers in glaciofluvial sands of Saalian and Weichselian ages. The uppermost and partly phreatic aquifer is separated from the deeper aquifer by up to 20 m thick glacial till layers, which locally pinch out. Hydraulic gradients of up to 0.5% are slightly steeper than reported for other NE German areas (**Figure 1**, Schafmeister and Darsow, 2004, Jordan and Weder, 1995; Jurasinski et al., 2018).

Based on the regional flow dynamics, ground water is entering the WB area from 3 hydraulic height maxima, situated at least 10 km away from the WB (Hennig and Hilgert, 2007). Within the catchment area (about 200 km^2), a lake Mühlenteich and other small streams act as routes of surface water flow into the WB.

The Mecklenburg Western-Pomeranian mean annual ground water recharge is about 123 mm/a, estimated by Hilgert (2009) and Hennig and Hilgert (2007). In combination with a mass balance approach, this leads to a rough daily SGD estimation of 60.000 m^3 to the WB (Schafmeister and Darsow, 2004). Ground water recharge rates in the western part of the WB are lower compared to the SE part (Hilgert, 2009; LUNG, 2009).

Ship and boat based fieldwork took place during the spring and summer of 2019. Meteoric water inputs to WB during this period made up 6% of the annual precipitation 548 mm - Germany Weather Station - Wismar (DWD, 2020).

No large rivers drain into WB, but streams such as the Wallenstein located in the eastern part of the coast and the Tarnewitzer on the western part contribute to the fresh water inputs. The average discharge of both streams based on 10-years data are 0.76 and 0.39 $m^3\ s^{-1}$ respectively (Stalu-MV, 2019). In addition to these streams, smaller ones are also present, however, no hydrologic data are available for them.

Sampling Strategy

Sampling in the WB was performed using RV LITTORINA (L19-06) between 20 and 25 May, 2019. Surface water samples were collected at 47 sites spanning the whole bay (**Figure 1**), and additional bottom water samples at four sites (**Supplementary Figure S1**). For sampling in shallow waters (<5 m) a rubber boat was used (20 sites). At six sites, short sediment cores were retrieved for pore water and sediment analyses (**Figure 1**). The coordinates of all sites in the WB are compiled in **Supplementary Table S1**.

At sites exceeding water depths >3 m, CTD profiles were obtained and surface water samples (1 m) were sampled using a submersible pump. The water was pumped through a filter cartridge (1 µm pore size) into 100 L barrels. Water subsamples were taken via syringe and filtered (0.45 µm, cellulose acetate disposable filters, Carl Roth) for analyses of major and trace elements, dissolved inorganic carbon (DIC), $\delta^{13}C_{DIC}$, and stable isotopes of water ($\delta^{18}O$ and $\delta^{2}H$). Samples for DIC and $\delta^{13}C_{DIC}$ were filled without headspace into 12 ml Exetainer® tubes, previously cleaned with 2% HNO_3 washed, dried, and pre-filled with 100 µl saturated $HgCl_2$ solution. Samples for major and trace element analysis were filled into acid cleaned 2 ml reaction tubes and acidified with concentrated HNO_3 to 2 vol.% and samples for $\delta^{18}O$ and $\delta^{2}H$ analyses were collected in 1.5 ml vials glass sealed with a PTFE-coated septum cap. All samples were stored dark and cool until further analyses.

Water samples in the barrels were pumped, using a submersible pump through manganese-coated acrylic fibers at a flow rate of 1 L min^{-1} to quantitatively extract radium (Ra) isotopes. The fibers were washed to remove salts and partly dried for further measurements.

Short sediment cores were collected at six different sites in the WB (**Figure 1**) using a Rumohr-Lot (60 cm length, inner diameter: 10 cm). For pore water sampling, Rhizons (Rhizosphere Research Products, 0.12 µm pore size (Seeberg-Elverfeldt et al., 2005)) were inserted in pre-drilled holes of the plastic liner and attached to 10 ml plastic syringes. Salinity and pH of pore waters were

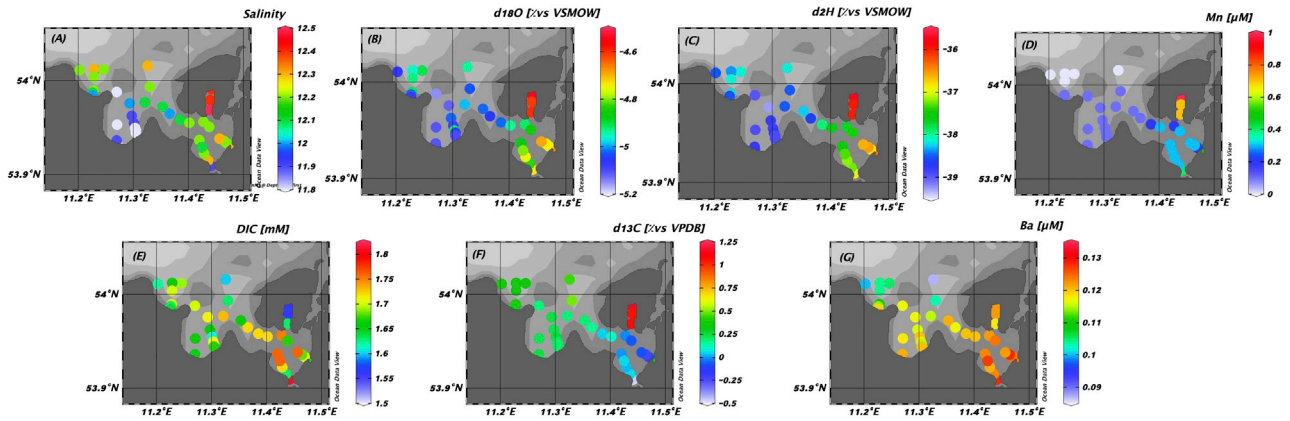

FIGURE 3 | Areal distribution of selected variables in surface waters of the Wismar Bay. Salinity **(A)**, $\delta^{18}O_{H2O}$ **(B)**, $\delta^{2}H_{H2O}$ **(C)** of water, dissolved Mn **(D)**, DIC **(E)**, $\delta^{13}C_{DIC}$ **(F)**, and Ba **(G)**.

measured immediately after recovery using a refractometer and hand-held pH meter (Schott handylab pH meter 11—calibrated with Mettler Toledo Buffer solutions), respectively. Pore water was fixed with 5% Zn-acetate solution for later analysis of total sulphide (H_2S) concentrations. Additional pore water samples were taken for major and trace elements, DIC, $\delta^{18}O$, and $\delta^{2}H$ of water, and preserved and stored as described above. Parallel sediment cores were (sites 10, 11, 15, 20, and 31), sliced at 2–4 cm intervals for geochemical analyses of sediments. Sediments at site 2 were sampled on the same core after pore water extraction. Sediment aliquots were transferred into 50 ml centrifuge tubes (Sarstedt) and kept frozen (−20°C) until further preparation.

Between July and August 2019 along the shoreline pore water samples were collected at five different sites in 0.4–1.8 m depth using push-point lances (MHE products) (**Figure 1**). In addition, four streams draining to the WB were sampled at the mixing zone with BS water. For major and trace elements, and stable isotopes analyses using the same methods as described for surface water of WB. In addition, samples for chloride (Cl) analysis were filled into 500 ml plastic bottles. pH, conductivity, and temperature were measured *in situ* using Schott handylab pH 11 and Schott handylab LF 11 devices. For Ra isotope measurements, 25 L of pore water was collected using a peristaltic pump, while 60 L of stream surface waters were collected and filtered through a 25 µm filter into pre-cleaned gallon containers for further filtration through the Mn fibers.

To identify the potential impact of SGD on coastal waters a pre-survey of Ra isotope distribution in surface water was carried in April 2021 along the shoreline between WB and Warnemünde (~50 km east of WB, **Figure 3**). Water samples for Ra measurements were taken at 23 sites, with 6 sites within WB and the remainder between WB and further east along the coastline (**Figure 3**). The sampling method is the same as described above.

The isotope-hydrochemical composition of ground waters emerging on a nearby coastal beach (Site Meschendorf–**Figure 1**) was considered for comparative purposes in the discussion of this study. The sampling was conducted in the same way as for the surface water campaign in the WB and took place in September 2018.

In addition, fresh ground water samples collected from monitoring wells located adjacent to the WB are presented for comparison purposes. Ground water sampling was carried out in 2014 and followed the protocol described by Jenner (2018). The ground water well at Poel Island (**Figure 1**) and the ground water well 2 are located in a confined aquifer with more than 10 m of soil layer above the filter screen. The other 3 ground water wells (1, 3, and 4) are located in an unconfined aquifer with sampling depths less than 5 m below the surface (Jenner, 2018).

Geophysical acoustic investigations of the subsurface sediments were carried out from July 29th to 31st 2019 using an Innomar SES96 parametric echo sounder mounted on the IOW research catamaran Klaashahn. Seismic data were collected at three frequencies, of which only the 8 kHz dataset is presented here. Results were corrected for ship movements using a motion sensor during data acquisition. The processing of the seismic data was done using Seismic Unix, which involved threefold stacking of the data for the signal to noise ratio improvement, and application of a time-varied gain. The time-depth conversion was calculated using a constant sound velocity of 1,500 m s^{-1}.

Analytical Methods

Water contents of the sediment samples were determined gravimetrically after freeze-drying (considering the water loss due to pore water extractions at Site 2). About 1 g of each sediment sample was pre-treated for grain size analysis by removing carbonate and organic matter using hydrochloric acid (HCl) and hydrogen peroxide, respectively to prevent the binding of the small particles. Grain size measurements in the range from 0.01 to 3.500 µm were performed using a Mastersizer 3,000 with a wet dispersion unit (Hydro EV; Malvern Panalytical). Grain size statistics (including the first mode) were calculated using the program GRADISTAT (Blott and Pye, 2001), applying the volume percentage data and a geometric graphical method modified after Folk and Ward (1957).

Freeze-dried sediments were analyzed for total carbon (TC), total nitrogen (TN), and total sulphur (TS) content with a CHNS Elemental Analyzer (Euro Vector EuroEA 3,052). The

combustion was catalyzed by V_2O_5, the resulting gaseous products were chromatographically separated and quantified via infrared spectrophotometry. Total inorganic carbon (TIC) was determined with an Elemental Analyzer multi-EA (Analytik Jena) after reaction with phosphoric acid 40% followed infrared spectrophotometry quantification of CO_2. The precision of the method were ±3, ±10, ±7.6, and ±4.3% for TC, TN, TS, and TIC respectively, using MBSS- (CNS) and OBSS-$CaCO_3$ (TIC) as in-house standards. The content of total organic carbon (TOC) was calculated from the difference of TC and TIC. The contents of total Mercury (Hg) were analyzed using a DMA-80 analyzer with a detection limit of about 0.15 μg kg^{-1}, as described by Leipe et al. (2013). The precision and accuracy of the measurement were ±8 and ±1.3%, respectively. The calibration was carried out with the 142R MBSS standards.

For the analysis of the acid extractable fraction of several metals (identified in the text with *) about 200 mg of freeze-dried and homogenized sediment was treated with 10 ml 0.5 M HCl agitated for 1 h (Kostka and Luther, 1994). The extracts were filtered with 0.45 μm disposable surfactant-free cellulose acetate membrane filters (Carl Roth), and analyzed by inductively coupled plasma optical emission spectrometry, ICP-OES (Thermo, iCAP, 7,400 Duo Thermo Fischer Scientific), after 10-fold dilution with 2% HNO_3 using external calibration and Sc as an internal standard. The international reference material SGR-1b (USGS) revealed precision and accuracy of better than 2.1 and 3.8%, respectively (Dellwig et al., 2019).

Major ions (Na, Mg, Ca, K, S) and trace elements (Ba, Fe, Li, Mn, Sr) in the water samples were analyzed by ICP-OES using matrix-matched external calibration (diluted OSIL Atlantic Sea water standard spiked with Ba, Fe, Li, Mn, and Sr) and Sc as internal standard. Precision and accuracy were checked with spiked SLEW-3 (NRCC) and were better than 4.7 and 7.6%, respectively.

Concentrations of H_2S were determined by the methylene blue method (Cline, 1969) using a Spekord 40 spectrophotometer (Analytik Jena). The chloride concentration of the water samples was determined by an electric potentiometric precipitation titration (Schott instruments), which utilizes the changing electrical potential difference of the solution by quantitative precipitation of Cl ions due to titration with 0.05 M $AgNO_3$. Analytical accuracy was constantly checked with the international reference standard OSIL Atlantic Seawater 35.

$\delta^{13}C_{DIC}$ values were determined as described by Winde et al. (2014) by means of continuous-flow isotope-ratio-monitoring mass spectrometry (CF-irmMS) using a Thermo Finnigan MAT253 gas mass spectrometer attached to a Thermo Electron Gas Bench II via a Thermo Electron Conflo IV split interface. Solutions were allowed to react for at least 18 h at room temperature before introduction into the mass spectrometer. The international calibration materials IAEA Ca carbonate standard and Solnhofer Plattenkalk were used for calibration of measured isotope ratios towards the V-PDB scale. $\delta^{18}O$ and $\delta^{2}H$ values of water were analysed with a CRDS system (laser cavity-ring-down-spectroscopy; Picarro L2140-I; Böttcher and Schmiedinger, 2021). The reference materials SLAP and VSMOW were used for calibration of measured isotope ratios towards the V-SMOW scale. All stable isotope results are giving in the δ-notation. The given '‰' values are equivalent to mUr (milli Urey; Brand and Coplen, 2012).

Ra isotopes (^{223}Ra, $t_{1/2}$ = 11.4d, and ^{224}Ra $t_{1/2}$ = 3.7d) were measured with radium-delayed coincidence counters (RaDeCC) (Moore and Arnold, 1996) within 3 days after sampling. After about a month, a further measurement was conducted for the determination of ^{224}Ra supported by ^{228}Th ($t_{1/2}$:1.9 years), this measurement is then subtracted from the initial ^{224}Ra to obtain the excess of ^{224}Ra activities ($^{224}Ra_{ex}$). Activities of ^{223}Ra, ^{224}Ra, and $^{224}Ra_{ex}$ were calculated and the expected error of the measurement is 12 and 7% for ^{223}Ra and ^{224}Ra respectively (Garcia-Solsona et al., 2008). The calibration of the detectors is done once a month using ^{232}Th with certificate activities. In this study, we do not discuss ^{223}Ra, but the data can be found in the **Supplementary Table S2**.

The isotope-hydrochemical analysis of the ground water from the wells was carried out by the department of "Strahlen und Umweltschutz" at the "Landesamt für Umwelt, Naturschutz und Geologie". As for methods used, all methods and DIN standards are given in **Supplementary Table S3**. The data was kindly provided by LUNG Güstrow and further details can be found at Jenner (2018).

Numerical Model

Steady-state modeling of pore water profiles was performed to assess the transport mechanism, i.e., diffusive or advective fluxes. The model further evaluates the essential geochemical reactions and the transformations rates. Net-release of a solute into the bottom water leads to positive transformation rates while net consumption results in negative transformation rates (Schultz, 2006).

Pore water sulphates (SO_4) and DIC concentration profiles were computed as a function of sedimentation rate, organic matter degradation, and diffusion rates using the reactive transport model described in (Meister et al., 2013). The following general equation was used:

$$\frac{\partial(\varphi C)}{\partial t} = -\frac{\partial(\omega\varphi c)}{\partial z} + \frac{\partial}{\partial z}\left(\frac{D_0}{\tau^2}\varphi\frac{\partial C}{\partial Z}\right) + \varphi\sum R_i \qquad (1)$$

where C is the concentration, t is time, ω is the sedimentation rate, z is the depth below seafloor, φ is the porosity, and D_0 is the diffusion coefficients corrected by tortuosity (τ^2), which was calculated according to Boudreau (1997) as $\tau^2 = 1–2\cdot\ln\varphi$. The mean sedimentation rate ω was taken as 2 mm yr^{-1} (Lampe et al., 2013) and an average porosity was taken as 0.88 derived from the sediment water content. The diffusion coefficients for SO_4 and DIC were calculated as 0.0236 and 0.0257 $m^2\,yr^{-1}$ respectively, based on the average temperature of 12°C and an average salinity of 13 (Boudreau, 1997).

Sources and sinks of SO_4 and DIC are stoichiometrically coupled to rates of organic carbon decay via the following simplified reaction for organoclastic sulphate reduction:

$$SO_4^{2-} + 2CH_2O \rightarrow HS^- + 2HCO_3^- + H^+ \qquad (2)$$

The organic matter decay rate R_G was followed by the reactive continuum (RC) model of Boudreau and Ruddick (1991).

$$R_G(t) = -\nu(a+t)^{-1}G(t) = -\frac{\nu a^{\nu}}{(a+t)^{\nu+1}}\frac{\rho_s(1-\varphi)G_0}{100\varphi M_C} \quad (3)$$

where the free parameters and a ν determine the shape of the initial distribution of organic matter reactivity. The parameter a describes the average life-time of the more reactive components of the spectrum whereas ν defines the shape of the distribution. The dry density of the sediment is ρ_s (ρ_s = 2.6 g cm^{-3}), M_C is the molecular weight of carbon (M_C = 12) and G_0 is the initial TOC upon sedimentation (wt%). Thus, the SO_4 reduction and DIC production rate can be given by $0.5R_G$ and R_G, respectively.

The isotopic composition was calculated from the measured ratios R and referred to the VPDB according to Hoefs (2018):

$$\delta^{13}C = \left(\frac{Rsample}{R_{VPDB}} - 1\right) \cdot 1000 \quad (4)$$

The absolute concentrations of [^{13}DIC] and [^{12}DIC] were computed by separated reaction-transport equations (**Eq. 1**) for each isotope. Negligible carbon isotope fractionation was assumed during organoclastic sulphate reduction (cf. Claypool and Kaplan, 1974). Therefore, this source of inorganic carbon was assumed to show the same isotopic composition as the organic source.

Initial conditions were 0 mM SO_4 and DIC at all depths. The computer domain was set to be 50 cm. The Dirichlet boundary condition was applied at both the sediment/water interface (z = 0 cm) and bottom (z = 50 cm) according to the observed data. All parameters used in the model are listed in **Supplementary Table S4**.

Data Presentation

The figures presenting the vertical profiles were created using Sigma Plot 10.0 software (Systat Software, Inc., United States). The concentration maps were plotted using Ocean Data View (Schlitzer, 2001). The study area map was created using the Qgis development Team.

RESULTS

Results of all chemical elements measured in the Wallenstein stream, western streams, beach pore water, fresh ground water from the wells, fresh surface water from springs in Meschendorf are listed in **Table 1**. To place these data in a context, the data of surface water and pore water from the WB were also compiled in this table. The parameters of these different waters were plotted against salinity to assess the behavior of the parameter along the salinity gradient and the contribution of mixing and biogeochemical processes (**Supplementary Figure S2**).

Water Composition

Surface Waters in the Wismar Bay

The salinity of the WB surface waters ranged between 11.8 and 12.5 (**Figures 3A**), which is in the range of previously observed (Prena, 1995). The WB water column was well mixed, showing a slight salinity increase in bottom waters at some sites (**Supplementary Figure S3**). All conservative elements followed expected trends by covarying with salinity.

The δ^2H_{H2O} and $\delta^{18}O_{H2O}$ varied between −35.7 and −39.3‰ and between −4.5 and −5.2‰, respectively. Heavier isotopic compositions were found in the sheltered eastern part of the bay, mainly near Poel Island. Towards the western part of the WB, the isotope values were lighter, but show a trend of decreasing values close to the coastline (**Figures 3B,C**).

In surface waters, DIC ranged from 1.5 to 1.8 mM (**Figure 3E**) and $\delta^{13}C_{DIC}$ varied between -0.5 and 1.1‰ (**Figure 3F**). We found a W-E trend increasing concentrations in DIC and an inverse relationship between concentrations and its stable isotope composition. Only the waters close to Poel Island showed the lowest concentrations and the highest $\delta^{13}C_{DIC.}$

The concentrations of manganese (Mn) and barium (Ba) varied between 0.03 and 0.1, 0.07, and 0.1 μM, respectively, (**Figure 3D,G**). The eastern area was characterized by higher concentrations of Mn and Ba compared to the western parts (**Figure 3E**).

The activities of $^{224}Ra_{ex}$ ranged between 3 and 28 dpm 100 L^{-1} with an average of 7 L dpm 100 L^{-1}, presenting also higher activities in the eastern area. The site located in open BS waters presented a ^{224}Ra activity of 1.5 dpm 100 L^{-1} (**Figure 2**).

Streams

The Wallenstein stream discharges into the eastern part of the bay and showed $\delta^{18}O_{H2O}$ and δ^2H_{H2O} values of −4.0‰ and −33.2‰, respectively, which were heavier than the other streams in the western part of the WB. All isotopic compositions plot below Local Meteoric Water Line (LMWL) established for the southern BS at Warnemünde (**Figure 4**) in contrast with the results for ground waters in the WB region that fall on LMWL (**Table 1**; **Figure 4**).

For a general characterization, the hydrochemical composition of the investigated waters is compiled in a Piper diagram (Piper, 1944) (**Figure 5**). Most of the streams can be characterized as Na-Cl, and one of them as CaMg-HCO_3 waters (**Figure 5**), with the Na-Cl type being impacted by mixing with BS water at the sampling site.

The western streams were enriched in DIC compared to the Wallenstein stream. The DIC concentration in the western streams reached 5.8 mM and the $\delta^{13}C_{DIC}$ values were around −13.2‰ whereas the Wallenstein stream had a concentration of 2.5 mM and a $\delta^{13}C_{DIC}$ value of 6.5‰.

The activities of $^{224}Ra_{ex}$ in the western streams (salinities 0.1–1.8) discharging to the western WB ranged from 7 to 24 dpm 100 L^{-1}, which is within the range of the activities measured in the WB surface waters. The activities for the Wallenstein stream were found to be slightly higher (36 dpm 100 L^{-1}).

Ground Water

Ground waters from the WB catchment are characterized by a water isotopic composition ranging from −8.6 to −8.3‰ ($\delta^{18}O_{H2O}$) and −58.8 to −56.7‰ (δ^2H_{H2O}), similar to the composition of the ground water escaping at the Site Meschendorf, which showed average values of −8.5 and 58‰ respectively (**Table 1**- springs; **Figure 4**).

TABLE 1 | Average, minimum, maximum, and number of samples of the WB surface water (WB), Wallenstein stream, small streams, beach pore water (PW), ground water (GW) from the wells near Wismar, GW from a well in Poel Island, springs located close to Wismar, sediment pore water (PW). The pore waters from the beach and from Wismar were extrapolated to 1 mM Na, which is the concentrations found in the fresh ground waters, and termed as central SGD and beach SGD.

Variables	Unit	WB	Wallenstein stream	Small streams	Beach pore water	GW well 1	GW well 2	GW well 3	GW well 4	GW well 5	Springs Meschendorf	PW st. 10 and 11	PW st. 2, 15, 20 and 31	Central SGD	Beach SGD
Salinity		12.1	7.2	1.7	5.5						0.1	13	14		
		11.8/ 12.6 (46)	(1)	0.1/1.8 (3)	3.1/10.2 (5)						0.1/0.3 (6)	1/15 (30)	12–17 (57)		
Cond.	mS. cm^{-1}		12.6	1.4	9.7	0.8	0.7	0.7	1.0	0.7	0.8				
			(1)	0.8/3.6 (3)	5.7/17.4 (5)	(1)	(1)	(1)	(1)	(1)	0.6/1.1 (6)				
pH		8.3	7.9	8.2	7.38	7.2	7.4	7.3	7.0	7.3	7.3	7.7	7.5		
		8.2/9.0 (17)	(1)	8.1/8.7 (3)	7.1/7.8 (5)	(1)	(1)	(1)	(1)	(1)	7.1/7.4 (6)	7.0/8.2 (30)	7.1/8.3 (57)		
Temp.	°C	14.2	23.7	21.0	20.3	10.2	10.2	10.2	10.9	10.0					
		11.7/20.0 (46)	(1)	16.5/23.5 (3)	19.9/24.7 (5)	(1)	(1)	(1)	(1)	(1)					
DIC	mM	1.67	2.5	4.9	8.6		6.1	5.5		5.4	6.1	7.1	3.5	6.4	13.4
		1.51/1.80 (49)	(1)	4.3/5.8 (3)	4.0/9.4 (5)	(1)	(1)	(1)	(1)	(1)	5.50/6.70 (6)	1.49/ 16.38 (29)	1.51/13.57 (55)	(1)	13.30/13.39 (2)
$\delta^{13}C_{DIC}$	‰ VPDB	0.21	-6.46	–13.23	–15.34	–13.77		–13.79	–14.24		–13.75	–9.29	–6.59	–6.63	–26.30
		–0.46/1.15 (49)	(1)	–13.92/ –10.95 (3)	–17.52/ –8.56 (5)	(1)	(1)	(1)	(1)	(1)	–14.4/–13.61 (2)	=–14.4/ 0.1 (29)	–13.4/0.2 (55)	(1)	–26.50/–26.10 (2)
$\delta^{18}O_{H2O}$	‰ VSMOW	–5.0	–4.0	–7.4	–6.1	–8.4	–8.3	–6.7	–8.4	–8.6	–8.5	–4.9	–4.78	–8.5	–7.14
		–5.2 /–4.5 (49)	(1)	–7.3/ –8.1 (3)	– 7.2/–5.2 (5)	(1)	(1)	(1)	(1)	(1)	–8.7/– 8.4 (4)	–7.2/–4.4 (29)	–5.15/–3.9 (55)	(1)	–8.34/6.26 (5)
$\delta^{2}H_{H2O}$	‰ VSMOW	–38.2	–33.2	–52.3	–43.8	–58.0	–56.7	–48.9	–57.3	–58.8	–57.7	–37.7	–36.4	–56.6	–49.4
		–39.3/–35.7 (49)	(1)	–55.4/ –51.5 (3)	–49.4/–39.3 (5)	(1)	(1)	(1)	(1)	(1)	–58.8/–57.2 (4)	–50.2/ 33.8 (29)	–39.5/–29.5 (55)	(1)	–55.35/–44.74 (5)
Cl	mM		124.5	25.1	74.3	1.21	1.30	0.79	0.99	1.32	0.53				
			(1)	1.45/26.30 (3)	39.40/ 165.09 (5)	(1)	(1)	(1)	(1)	(1)	0/0.66 (3)				
Na	mM	162.2	98.4	23.50	66.9	0.7	2.2	1.0	0.8	0.83	1.03	165.6	176.7	1.0	1.0
		150.5/169.2 (49)	(1)	1.35/36.5 (3)	23.7/142.4 (5)	(1)	(1)	(1)	(1)	(1)	0.9/1.1 (5)	30.9/ 207.4 (23)	148.7/244.2 (55)	(1)	(5)
Mg	mM	18.3	11.4	2.9	9.2	0.5	0.6	0.4	0.6	0.7	0.7	18.64	19.0	0.0	0.3
		17.1/19.9 (49)	(1)	0.7/5.6 (3)	3.0/16.9 (5)	(1)	(1)	(1)	(1)	(1)	0.6/0.9 (5)	2.4/21.8 (23)	16.7/24.2 (55)	–1	0/7.6(5)
Ca	mM	4.0	3.3	2.9	8.0	3.7	2.1	2.5	4.0	3.1	3.5	4.2	4.5	2.4	10.1
		3.7/4.1 (49)	(1)	2.6/3.1 (3)	2.8/14.2 (49)	(1)	(1)	(1)	(1)	(1)	2.7/4.8	3.0/5.3 (23)	3.7/5.6 (55)	(1)	2.6/38.9 (4)
K	mM	3.5	2.2	0.9	1.7	0.0	0.1	0.3	0.3	0.1	0.1	3.7	3.87	0.6	0.3
		3.3/3.7 (49)	(1)	0.1/2.2 (3)	0.6/3.4 (5)	(1)	(1)	(1)	(1)	(1)	0.1/ 0.2 (5)	1.2/4.2 (23)	3.3/5.4 (55)	(1)	0/2.7 (5)
SO_4	mM	9.9	5.8	0.7	4.4	0.6	0.2	0.5	2.3	1.0	1.5	0.0	10.0	0.0	1.0
		9.2/10.4 (49)	(1)	0.6/2.2 (3)	0.8/8.9 (5)	(1)	(1)	(1)	(1)	(1)	1.1/2.7 (5)	0/10.25 (23)	5.3/12.1 (55)	(1)	0/3.4 (5)
Si	µM	6.1	0.1	0.4	0.4						0.4	622.3	258.5	887.3	0.0
		4.4/10.6 (49)	(1)	0.2/0.5 (3)	0.1/0.5 (5)						0.3/0.4 (5)	6.8/ 756.28 (23)	6.2/685.5 (55)	(1)	(3)
P	µM	0	9.9	13.5	11.3						4.2	76.8	38.8	22.0	13.7
		0.0/0.0 (49)	(1)	6.6/284.7 (3)	4.1/22.6 (5)						2.3/5.3 (5)	1.7/269.4 (20)	4.2/89.2 (55)	(1)	4.9/185.0 (5)
Ba	µM	0.1	0.4	0.2	1.1	0.3	0.8	0.3	0.5	0.9	1.1	0.3	0.2	1.4	1.1
		0.1/0.1 (49)	(1)	0.2/0.6 (3)	0.2/2.9 (5)	(1)	(1)	(1)	(1)	(1)	0.8/2.0 (5)	0.12/1.79 (24)	0.1/1.3 (55)	(1)	0.4/7.7(5)
Fe	µM	0.1	1.6	1.1	1.3						55.6	0.7	0.3	10.2	2.1
		0.1/1.8	(1)	0.4/2.1 (3)	0.2/2.1						44.7/124.1 (5)	0.1/624.2 (23)	0.0–5.2 (55)	(1)	1.1/3.5 (5)
Li	µM	8.6	6.4	2.9	8.3						2.0	9.2	9.9100	5.8	4.8
		8.2/9.1 (46)	(1)	2.1/3.0 (3)	2.3/9.9 (5)						1.5/2.1 (5)	6.9/11.5 (23)	8.4/ 13.2 (55)	(1)	2.4/13.0 (5)
Mn	µM	0.1	3.5	2.6	12.0	0.0	0.0	0.0	0.0	0.0	3.0	2.3	1.9	4.2	17.4
		0.0/1.5 (46)	(1)	0.7/4.3 (3)	1.5/24.4	(1)	(1)	(1)	(1)	(1)	2.8/4.6 (5)	0.2/58.2 (23)	0.1/9.5 (55)	(1)	1.7/44.5 (5)
Sr	µM	32.0	21.6	9	28.7						5.6	34.2	35.6	6.9	9.9
		29.9/33.3 (49)	(1)	6.4/13.9 (3)	8.4/34.0 (5)						5.0/9.7 (5)	14.01/ 40.7 (23)	31.0/ 44.3 (55)	(1)	4.6/39.0 (5)
^{224}Ra	dpm $100L^{-1}$	8.01	36.2	15.6	362.2										
		2.8/27.4 (49)	(1)	6.8/24.3 (3)	25.8/ 547.1 (5)										
^{223}Ra	dpm $100L^{-1}$	0.9	0.9	0.4	10.6										
		0/1.7 (26)	(1)	01/0.6 (3)	0.5/18.0 (5)										
$^{224}Ra_{ex}$	dpm $100L^{-1}$	7.3	34.9	15.4	350.6										
		2.3/26.5 (49)	(1)	6.3/23.7 (3)	17.6/530.0 (5)										

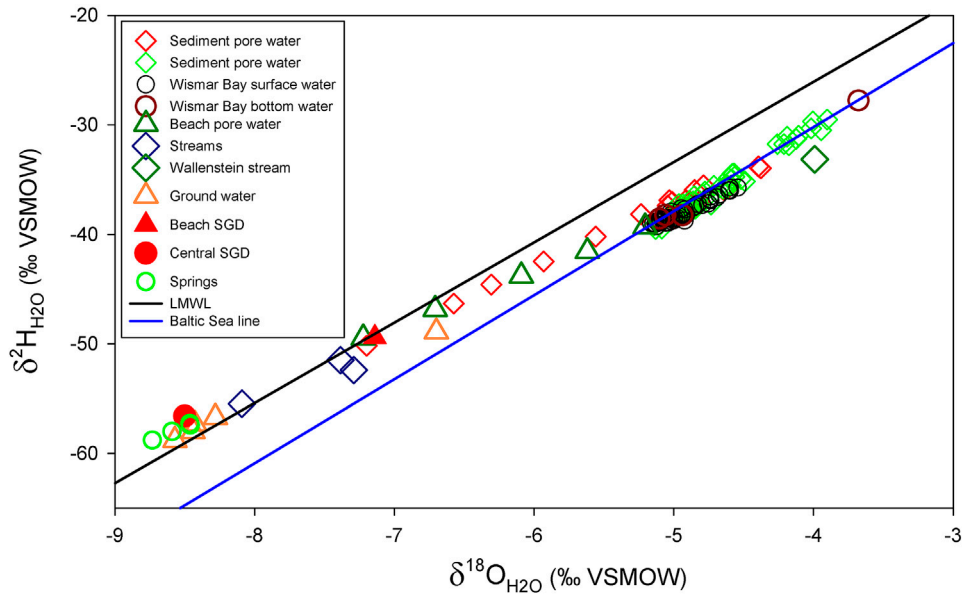

FIGURE 4 | Scatter plot of δ^2H_{H2O} versus $\delta^{18}O_{H2O}$ for sediment porewaters, both impacted (red diamonds) and non-impacted by SGD (green diamonds), Wismar Bay surface (black circles) and bottom (brown circles) waters, beach porewater (green triangles), streams (blue diamond), river (large dark green diamond), ground water (yellow triangle), Beach porewater extrapolated to 1 mM Na called Beach SGD (filled red triangle). The Local Meteoric Water line (LMWL) and the Baltic Sea surface water line from (Böttcher et al., 2020) are also presented.

The hydrogeochemical ground water composition in the region around the WB and of Meschendorf can be classified as Ca-Mg-HCO_3 type (**Figure 5**). Based on the classification scheme by Löffler et al. (2010) it can be further characterized as a relatively young confined ground water.

Sediment Pore Water at the Beachline of Wismar Bay

Salinities of beach pore waters ranged between 3 and 10 (**Table 1**), representing different relative mixtures between fresh (salinities <1) and brackish waters (salinities of the WB: 11.8–12.5). Metabolites were enhanced when compared with the composition of the WB surface water, streams, and fresh ground waters around the WB (**Supplementary Figure S2**).

The water isotope data varied from −7.2 to −5.2 ($\delta^{18}O_{H2O}$) and −49.4 to −39.3‰ (δ^2H_{H2O}), reflecting also a mixture between two different endmembers (**Figure 4**).

The average $^{224}Ra_{ex}$ activity was 351 ± 188 dpm 100 L^{-1} (n = 5), which is one order of magnitude higher than those found in the surface waters from either WB or in the streams (**Table 1**).

Sediment Pore Water in the Wismar Bay

The downcore variation in the pore waters composition from six sediment sites in the WB is presented in **Figure 6** as a function of sediment depths. Sites 2, 15, 20, and 31 are presented separately from sites 10 and 11.

Sediments at sites 2, 15, 20, and 31 showed pore water profiles with constant salinity, except for a slight maximum at around 6 to 15 cmbsf, (**Figure 6A**). At Site 10 and in particular Site 11 (**Figure 1**), a strong downcore decrease in salinity was found. Relative to the bottom water conditions, the pore water salinities at Site 10 decreased by about 30% at 40 cmbsf. At the same depth, the salinity gradient at Site 11 reached essentially fresh water conditions (**Figure 6A-2**). In agreement with the salinity changes, the other conservative elements (Na, Mg, and K) also decreased with depth.

The δ^2H_{H2O} and $\delta^{18}O_{H2O}$ isotope values of the pore water at sites 2, 15, 20, and 31 varied from −39.5 to −29.5‰ and −5.1 and −3.9‰ respectively (**Figures 6B,C**). Due to the freshening by ground water at depth, the down core variations at sites 10 and Site 11 are much more pronounced, −50.2 and −36.9‰ (δ^2H_{H2O}) and −7.2 and −4.9‰ ($\delta^{18}O_{H2O}$), and at 40 cmbsf at sites 11 and 10, respectively (**Figures 6B-2,C-2**).

All pore waters were enriched in metabolites when compared to the bottom waters (**Table 1**), with increase concentrations at depth. A pronounced maximum concentration in the top 10 cmbsf was found at Site 11 (**Figures 6K-2–M-2, O-2**).

Pore water concentrations of SO_4 at the sediment-water interface were between 8 and 12 mM and decreased with depth, reaching 2 mM at most sites, and reaching even complete depletion at the base of Sites 10 and 11 (fresh water influenced sites) (**Figure 6I-2**). H_2S was determined at all sites showing net accumulation below about 16 cmbsf. At site 11, no H_2S accumulation was observed (**Figure 6J-2**).

The concentrations of DIC increased with depth up to 16 mM at all sites except for Site 11 where again a maximum was found in 10 cmbsf (**Figure 6-O2**). The increase in DIC concentrations was associated with a decrease in $\delta^{13}C_{DIC}$ values (**Figure 6P-2**).

Results from the modeling downcore profiles of SO_4, DIC, and $\delta^{13}C_{DIC}$ were indicated by dashed lines in the panels I, I-2, O, O-2, P, P-2 of **Figure 6**. The corresponding fluxes and accumulated mineralization rates in depth intervals of 10 cm are given in

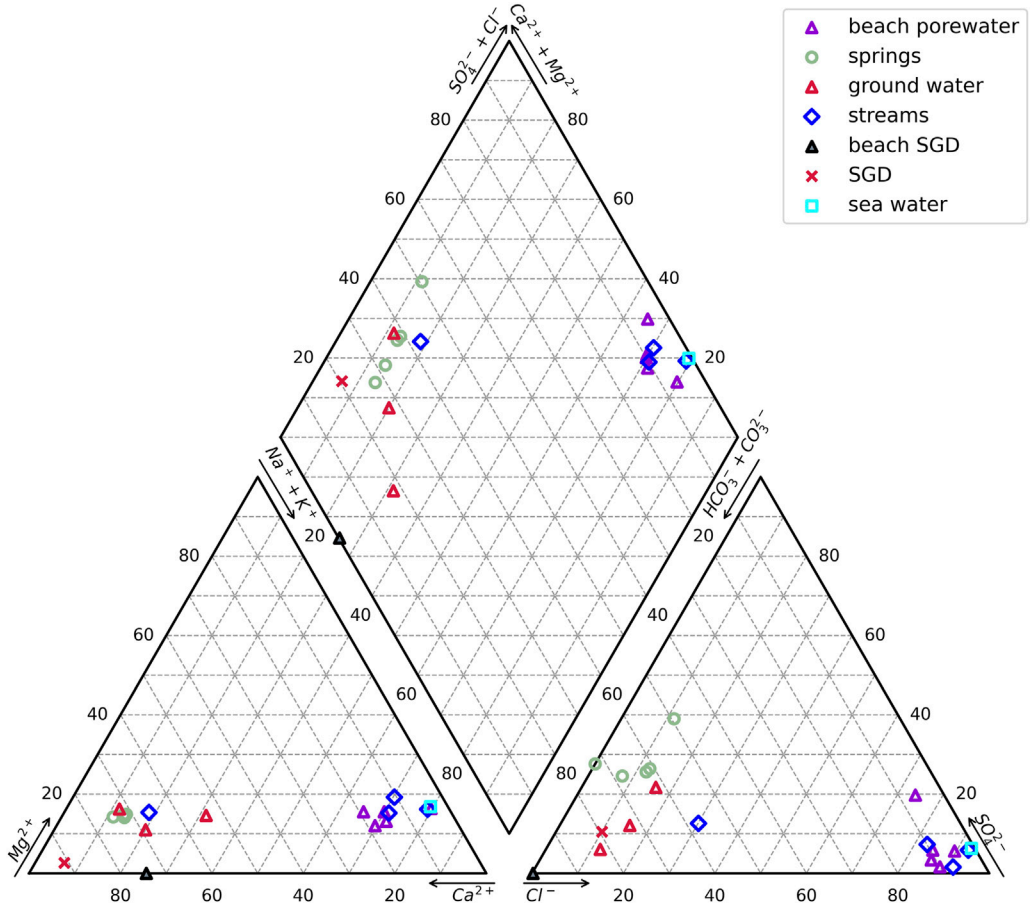

FIGURE 5 | Piper diagram of the major ions of the Wallenstein stream and western streams (blue diamond), springs (green circle), fresh ground water (red triangle), beach porewater (purple diamond) and sea water of Wismar Bay (turquoise square), extrapolated beach porewater (beach SGD—black triangle) and porewater of site 11 (SGD—red cross) to 1 mM Na.

Table 2. The modeled SO_4 fluxes both in the top and bottom sediment are positive and similar at all the sites. In contrast, the modeled DIC fluxes are negative, except at Site 11 which shows positive fluxes. In addition, the results of the model show that in the first 10 cmbsf of the majority of the sites there is a high OM accumulation, especially in Site 11, which is caused by a reactive metal oxide other than sulphate reduction. To verify the additional OM mineralization rate by reactive metal oxide on this site, different mineralization rates at 6–10 cm were tested (**Supplementary Figure S4**). It becomes obvious that an enhanced OM mineralization rate is required to fit the $^{13}C_{DIC}$ values.

Sediment Composition

Sediment Geochemistry

All sediment cores comprised a dark gray to black color with muddy texture covered by a brown fluffy layer on top.

Grain-size analyses show an uni-to bimodal distribution in the upper sediment. The vertical grain-size characteristics represented here by the first mode are given in **Supplementary Figure S5**. The samples first mode ranges between 8 and 100 µm. Fine to medium silt dominate at sites 10 and 11 (<40 µm) and at the surface of site 2 (subsurface), while sites 15 and 31 consist of coarse silt with a second mode around 8 µm. At site 20, in the southeastern part of WB, sediments consist of very fine sand. At sites 10 and 11 grain-size becomes finer with depth, whereas the mean grain-size increases at the other sites. The water content of the sediments ranged between 44 and 87% and generally decreased with sediment depth (**Supplementary Figure S5**).

The total organic carbon (TOC) contents ranged from 1 to 8% dwt. Organic matter-rich sediments (TOC >4 %wt.) were found at sites 10, 11, and 31, whereas sediments at other sites contained less TOC (**Figure 7C**). The molar TOC/TN ratios varied between 6 and 12 (**Figure 7D**) with increasing ratios with sediment depth. Total sulphur (TS) contents ranged from 0.3 to 2.4 wt. % (**Figure 7B**), typical for marine sediments (**Figure 8**) (Berner and Raiswell, 1983). Reactive Fe and Mn were generally pronounced in the top layers and mostly decreased at larger depths (**Figure 9**). Site 11 was characterized by the relatively highest values.

In brackish-marine sediments, microbial sulphate reduction limited by the availability of OM (Berner, 1980) which may be reflected by a positive co-variation of TOC with pyrite sulphur as found for Holocene sediments (Berner, 1982). The TS contents (taken here as a measure for pyrite sulphur) found in the shallow sediments of WB are positioned on or below the relationship

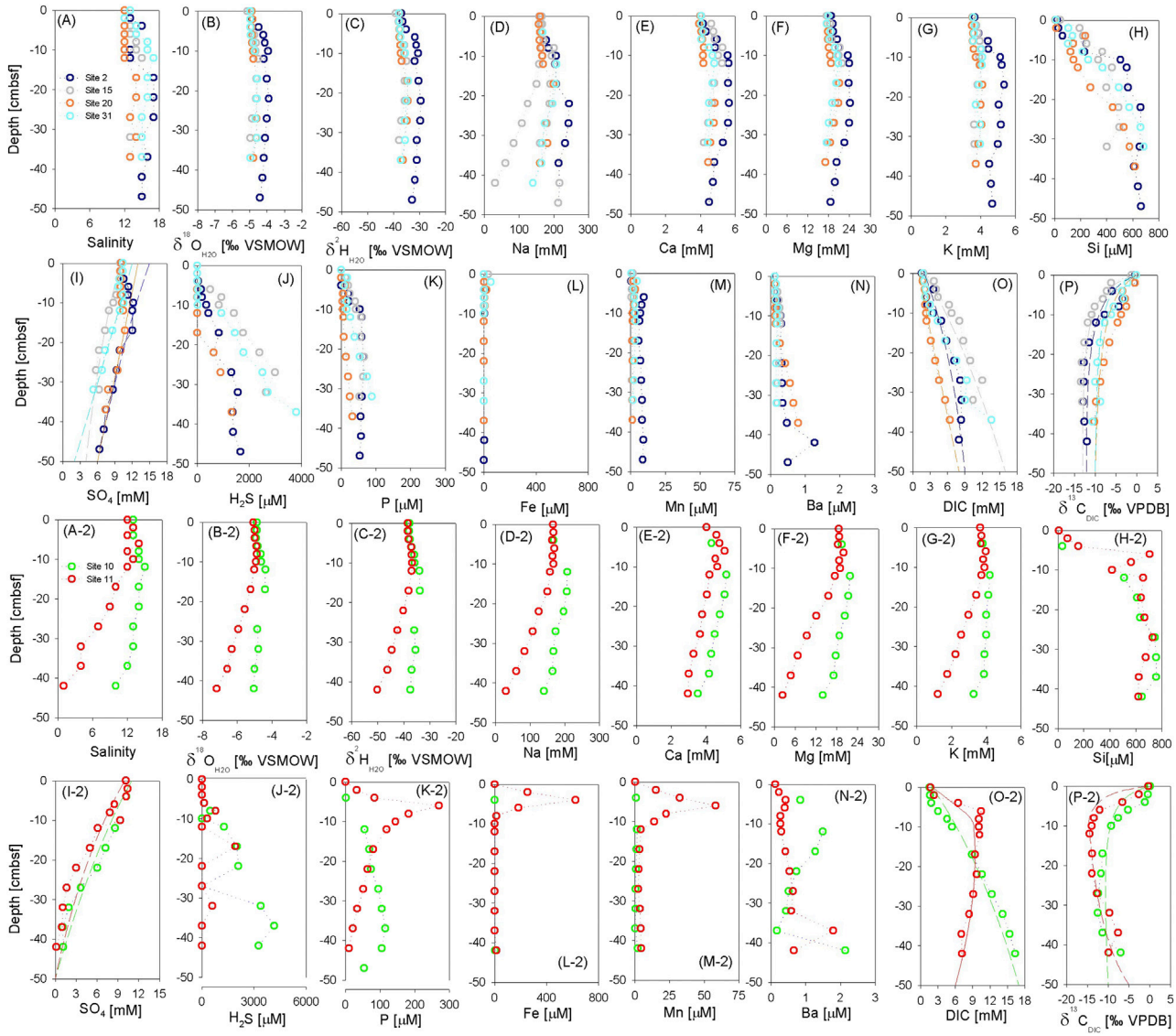

FIGURE 6 | Pore water profiles in sediment cores from WB showing salinity **(A)**, $^{18}O_{H2O}$ **(B)**, $^{2}H_{H2O}$ **(C)**, and different dissolved components Na **(D)**, Ca **(E)**, Mg **(F)**, K **(G)**, Si **(H)**, SO_4 **(I)**, H_2S **(J)**, P **(K)**, Fe **(L)**, Mn **(M)**, Ba **(N)**, DIC **(O)**, $^{13}C_{DIC}$ **(P)**, of sites 2, 15, 20, and 31. The sites impacted by freshening at depth are presented in the panels: salinity **(A-2)**, $^{18}O_{H2O}$ **(B-2)**, $^{2}H_{H2O}$ **(C-2)**, and different dissolved components Na **(D-2)**, Ca **(E-2)**, Mg **(F-2)**, K **(G-2)**, Si **(H-2)**, SO_4 **(I-2)**, H_2S **(J-2)**, P **(K-2)**, Fe **(L-2)**, Mn **(M-2)**, Ba **(N-2)**, DIC **(O-2)**, $^{13}C_{DIC}$ **(P-2)**. The additional dashed lines in the panels I, I-2, O, O-2, P, P-2 are the diagenetic modeling results.

proposed for siliciclastic sediments deposited beneath an oxygenated water column (**Figure 8**) (Berner, 1982).

The typical anthropogenic contaminants as Hg and acid-extractable lead (Pb*), showed pronounced variations reaching maximum contents of 156 µg kg^{-1} and 60 mg kg^{-1}, respectively, mostly in the shallower part of the cores (**Figure 9**). Here, relatively similar concentrations may be related to bioturbation, probably caused by different activities of macrozoobenthos (Lipka et al., 2018b; Gogina et al., 2018). At Site 11, lateral sediment supply from the flanks of the channel, sediment redistribution caused by the channel excavation, and fresh water flow from below may have cause relative constant concentrations. At Site 11, both Hg and Pb* concentrations show no trend with depth.

Geophysical Characterization

The position of transects within WB are displayed in (**Figure 1**) and the results of the acoustic measurements are presented in **Figures 10**, **11**. In the western transect, a steep drop in the bathymetry from less than 3 m water depth to approximately 9 m water depth is observed (**Figure 10**). In shallow waters of 3 m water depth and less no subsurface structures can be recognized in the seismic data.

Directly below the seafloor at the base of the steep drop (near site 15), mostly acoustically transparent sediments with weak horizontal internal layering are deposited (S2). Within this unit, gas fronts prohibited further penetration of the acoustic signal, and are recognized along the profile by high acoustic turbidity. At

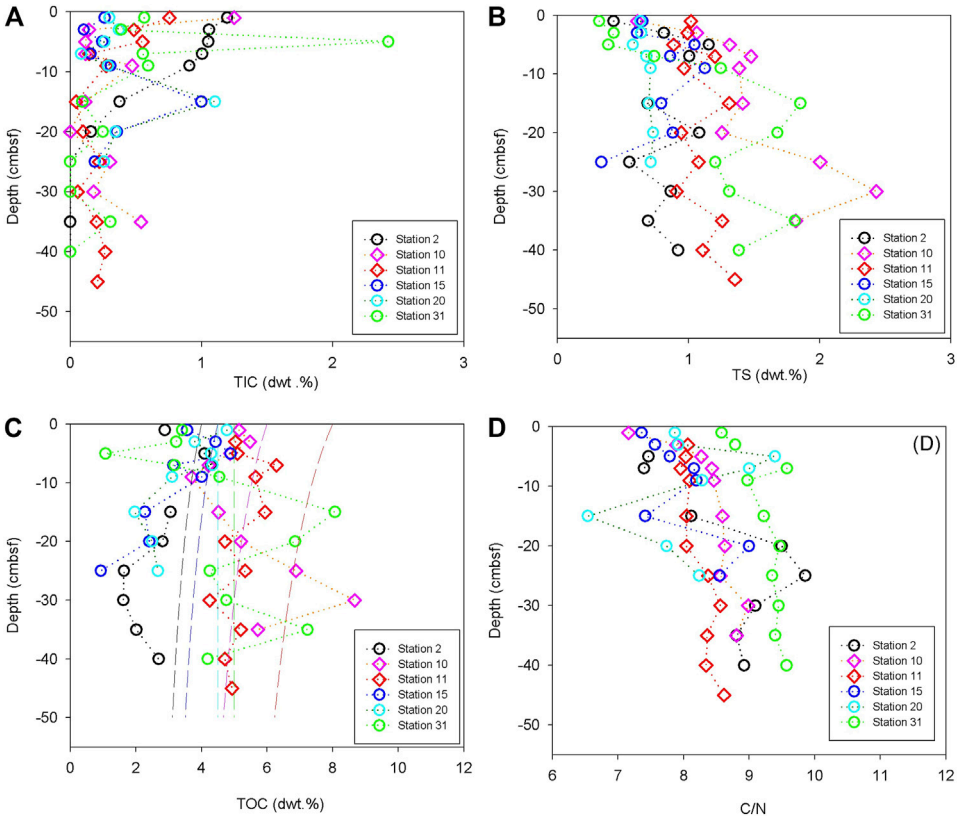

FIGURE 7 | Vertical profiles of the bulk geochemical parameters TIC **(A)**, TS **(B)**, TOC **(C)**, and C/N **(D)** ratios in sediments cores from the WB. The dashed lines in panel C (TOC) display the results from the diagenesis transport model (see discussion).

two locations (Site 13 and between sites 13 and 14), chimneys rise from the gas front to the seafloor. Between sites 13 and 15, the gas front was penetrated and the seismic units S3 and S4 can be observed. A distinct reflector is forming a low angle unconformable boundary of S3 with the overlying unit S2. Within unit S3, a faint and distorted internal lamination is observed. Unit S3 is separated from unit S4 by an unconformable high-amplitude reflector that is strongly undulating. Unit S4 is acoustically transparent and forms the base of acoustic penetration, corresponding to the onset of glacial deposits.

In the central WB, a channel dredged for ship traffic to approx. 10 m water depth is visible (**Figure 11**). At the flank of this artificial depression, seismic unit S1 is observed in the top meter of the subsurface. Based on the acoustic measurement, the unit has a chaotic texture but may be separates into sub-units by an unconformity (near site 31). A medium to high amplitude reflector separated unit S1 from S2, which again shows a weak, horizontal internal lamination with a thickness of up to 3 m. Along the majority of the profile, free gas fronts are observed at a depth of approx. 9 m. Near site 30, a gas chimney reaches the seafloor. Closer to the channel and on a perpendicular profile, unit S3 occurs with a thickness of approx. 1 m. Seismic unit S4, separated from the overlying units by a marked unconformity, forms the base of acoustic penetration.

DISCUSSION

Fresh Water in the Catchment Area and Inlets at the Margins of Wismar Bay

Fresh ground waters from the catchment in the southern part of the WB and from a well on Poel Island (**Figure 1**) display a water isotope composition positioned on the LMWL of Warnemünde (**Table 1**; **Figure 4**). These data are also close to the composition of ground waters escaping at beach spring in Meschendorf (**Figure 1**), which has been shown water of age about 30 years (Lipka et al., 2018a). The hydrogeochemical ground water composition of the majority of investigated wells and the springs fall into the field for relatively "young" ground waters (**Figure 5**).

The Wallenstein stream and the other western streams carry different isotope-hydrochemical signatures, thus representing different surface waters sources entering the southern WB.

The western streams showed a water isotopic composition and $\delta^{13}C_{DIC}$ signatures similar to those found in the well waters of the catchment area (**Table 1**). The slight shift towards heavier isotope values is likely the result of an impact by evaporation and CO_2 degassing when stream waters get in contact with the atmosphere (Michaelis et al., 1985; Clark and Fritz, 1997).

The Wallenstein stream, on the other hand, is enriched in heavy water isotopes and dissolved ions when compared to well waters

TABLE 2 | Modeled diffusive and advective fluxes of DIC and SO_4 and the accumulated OM mineralization rate for all the 6 sediment core sites. The fluxes and the rates are given in mmol m^{-2} d^{-1}.

	Advective and diffusion fluxes					
Sites	**2**	**10**	**11**	**15**	**20**	**31**
			Top (z= 0 cm)			
			SO4 flux			
Advective flux	0.07	0.05	0.05	0.05	0.06	0.06
Diffusive flux	1.18	1.55	1.66	1.66	0.62	0.89
Total flux	1.25	1.60	1.70	1.70	0.68	0.94
			DIC flux			
Advective flux	0.01	0.01	0.01	0.01	0.00	0.00
Diffusive flux	−1.46	−2.62	−4.30	−2.24	−0.68	−1.36
Total flux	−1.45	−2.61	−4.29	−2.22	−0.68	−1.36
			Bottom (z= 50 cm)			
			SO4 flux			
Advective flux	0.03	0.00	0	0.02	0.03	0.01
Diffusive flux	0.60	0.66	0.44	0.29	0.65	0.93
Total flux	0.63	0.66	0.45	0.31	0.68	0.94
			DIC flux			
Advective flux	0.04	0.08	0.03	0.08	0.04	0.07
Diffusive flux	−0.23	−0.81	1.01	−0.89	−0.72	−1.43
Total flux	−0.19	−0.73	1.04	−0.81	−0.68	−1.36
			Accumulated OM mineralization rate			
0-10 cm	0.44	0.66	3.70	0.49	0.00	0.00
10-20 cm	0.29	0.44	0.59	0.33	0.00	0.00
20-30 cm	0.22	0.32	0.43	0.24	0.00	0.00
30-40 cm	0.17	0.26	0.34	0.19	0.00	0.00
40-50 cm	0.14	0.21	0.28	0.16	0.00	0.00
0-50 cm	1.26	1.89	5.34	1.42	0.00	0.00

and western streams (**Figure 4**; **Table 1**). Besides the mixing with BS surface waters during the time of sampling, this could also be the result of surface water evaporation (e.g., Gat, 1996; Clark and Fritz, 1997) that took place during the origin of this stream in Lake Schwerin and a further crossing through Lake Mühlenteich before reaching the WB coastline (**Figure 1**).

The impact of stream waters on the composition of the WB surface waters is most pronounced in the western part of the bay. There the water isotopic composition decreased towards the coastline (**Figures 3B,C**), due to mixing between open BS water, containing heavier isotopes, and a fresh water component characterized by lighter isotopes. In addition, higher concentrations of DIC together with the depleted $\delta^{13}C_{DIC}$ found near the western coastline (**Figures 3E**) are probably related to fresh water sources (Winde et al., 2014). The surface water of the WB in the western part showed water isotopes values decreasing close to the coastline (**Figures 3B,C**), probably due to mixing between open BS water containing heavier isotopes, and a fresh water component characterized by lighter isotopes coming from the small streams located in this region. These streams showed a water isotopic composition similar to those found in the ground water recovered from wells near Wismar (**Table 1**, GW) and fresh water springs at Meschendorf (**Table 1**–springs). The slight trend to heavier isotopes is likely the result of an impact by evaporation and CO_2 degassing when stream waters become in contact with the atmosphere (Clark and Fritz, 1997). The $^{13}C_{DIC}$ isotopic signatures of the western streams are similar to the values in the ground water as well, which reinforces the idea that the streams are supplied by ground water from unconfined aquifers.

Within the western part of the WB, ^{224}Ra activities showed a decrease towards the open BS (**Figure 2B**). Since the ^{224}Ra activities in the streams were comparable to those measured in the surface water of the WB (**Figure 2**; **Table 1**), further sources may are contributing to the observed spatial patterns. Besides the ground water below the central part of the bay (see 4.3), which has not been analyzed for ^{224}Ra, the permeable sediments along the bay may act as a further fresh water and ^{224}Ra source to the WB. The pore water at the beach showed average $^{224}Ra_{ex}$ activities that were about one order of magnitude higher than the activities found in the surface water of WB. These findings, therefore, suggest, that SGD can enter the WB from the boundaries and contributing as a further source to the water balance of the WB.

Beach pore water consist of a mixture between fresh water and a brackish water component. To estimate the fresh water endmember the beach pore water compositions were extrapolated based on actual measurements and using Na as conservative mixing tracer (boundary conditions: average WB and 1 mM for the fresh water, which is the mean concentration found in the ground water wells). These values can be found in **Table 1**—Beach SGD. For the majority of the dissolved compounds a composition close to ground waters was found (**Table 1**). Only some non-conservative constituents, like DIC and Ca were enhanced in the estimated fresh water component, likely due to corrosion processes of carbonates present in the coastal sands (e.g., Smellie et al., 2008).

Although a ^{224}Ra gradient was not established in the eastern part of the WB (**Figure 2**), the generally higher activities in this part may indicate a source of ^{224}Ra. This source may originate from the exchange with pore water or resuspended sedimentary particles or SGD, besides the Wallenstein stream. Moreover, enhancement of Mn and Ba compared to the open BS surface water confirms strong benthic pelagic fluxes.

Tentative Radium Mass Balance for Wismar Bay

A mass balance is constructed, based on Rodellas et al. (2021), to estimate SGD in the WB. The Ra mass balance relies on the assumption that the most important Ra sources and sinks are in steady state, and then SGD can be evaluated by the difference of supply and removal according **Eq. 5**.

$$F_{SGD} * A_{SGD} + Q_{str}C_{str} + F_{sed} * A_{WB} = \lambda VC + Q_{out}C \qquad (5)$$

Where V and A_{WB} are the water volume (m^3) and surface area (m^2) of where samples were collected (**Figure 1**). We assume for the balance that SGD is taking place at 27 km of the shoreline and 10 m offshore (A_{SGD}). Q_{str} is the discharge from streams (m^3 d^{-}). We consider here the Wallenstein stream and the three western streams. Q_{out} is the water outflow to the open BS (m^3 d^{-1}) determined by using the water mass ages, the activity difference between WB and open-sea water and the volume of the study area. The water ager was calculated following (Moore and de Oliveira, 2008). C is the weighted average of $^{224}Ra_{ex}$ of the WB, determined by the $^{224}Ra_{ex}$ inventory. C_{str} are the mean concentrations of $^{224}Ra_{ex}$ in the surface water inlets (Bq m^{-3}). F_{sed} is the $^{224}Ra_{ex}$ diffusion from sediments. λ is the radioactive decay constant of ^{224}Ra. F_{SGD} is the fluxes of $^{224}Ra_{ex}$ per unit area associated with SGD (Bq m^{-2} d^{-1}), respectively. Terms used in the mass balance together with the units are summarized in **Table 3**.

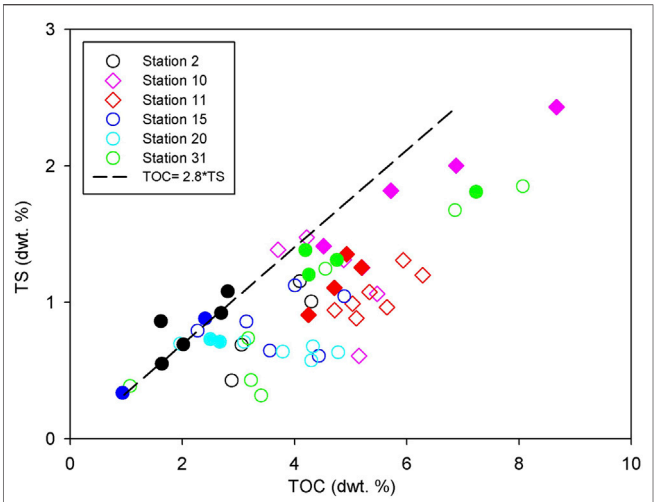

FIGURE 8 | Covariations of TS versus TOC including the relationship suggested for Holocene siliciclastic sediments (Berner, 1982). It is assumed that TS essentially consists in the investigated samples essentially of pyrite sulfur. Surface sediments <20 cmbsf are open symbols and >20 cmbsf are filled symbols.

Solving **Eq. 5** a $^{224}Ra_{ex}$ flux from SGD (F_{SGD}—**Table 3**) of 261.7 Bq m^{-2} d^{-1} was obtained.

This flux was converted into a water flow by dividing it by the $^{224}Ra_{ex}$ activities in different endmembers which were derived from four beach pore water samples with activities of 51, 65, 84, and 88 Bq m^{-3}. The resulting estimated volumetric SGD flow is 3.8 ± 0.7 cm d^{-1} (**Table 3**).

The estimated flow is higher compared to the flow obtained by (Schafmeister and Darsow, 2004). These authors applied a numeric ground water flow model (about 0.02 cm d^{-1}). This is due to the model only considering the fresh water component, whereas the Ra mass balance applied in the present study includes recirculated sea water. However, the SGD rate from WB is considered low when comparing to other SGD rates from different regions in the world, where SGD rates can reach up to 280 cm d^{-1} (Santos et al., 2021).

Benthic Processes and Submarine Fresh Water Source in the Central Wismar Bay

The composition of sediments investigated in the WB is typical for silty/muddy deposits along the North-German coastline

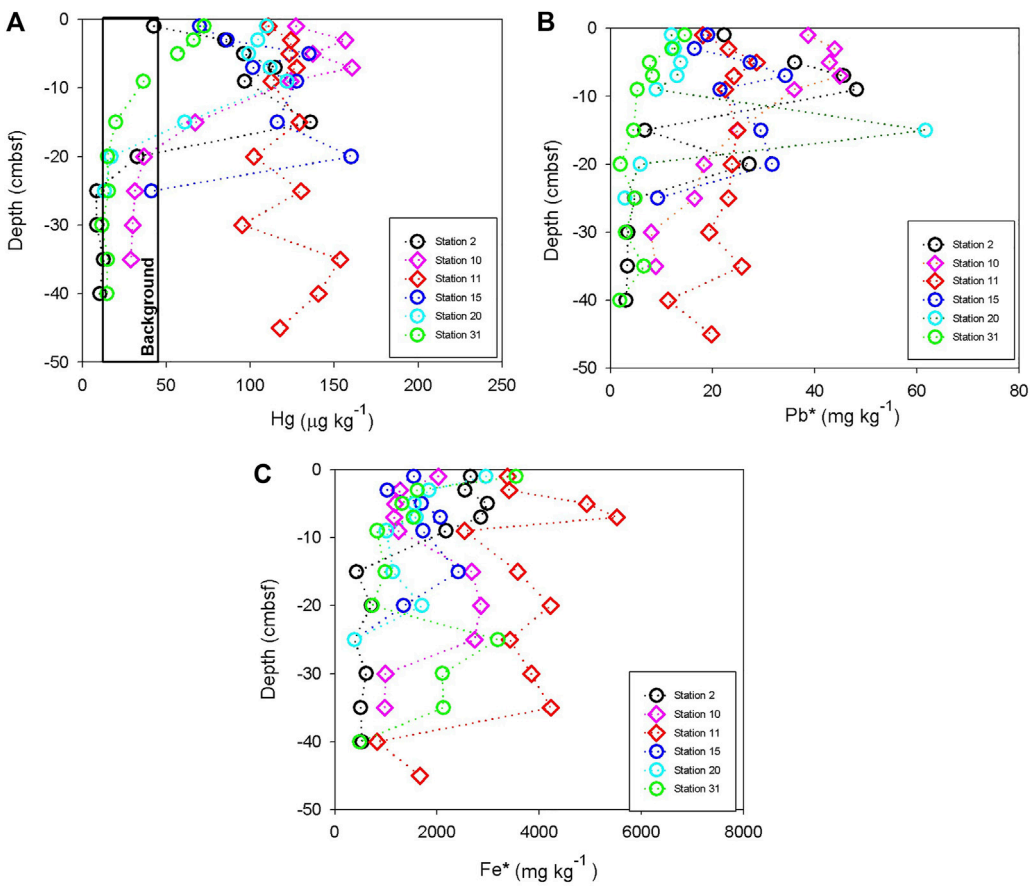

FIGURE 9 | Vertical profiles of the contents of total Hg, **(A)**, including the background level for Baltic Sea (Leipe et al., 2013), and Pb **(B)** and Fe **(C)** of sediment cores from WB. *HCl extractable fraction.

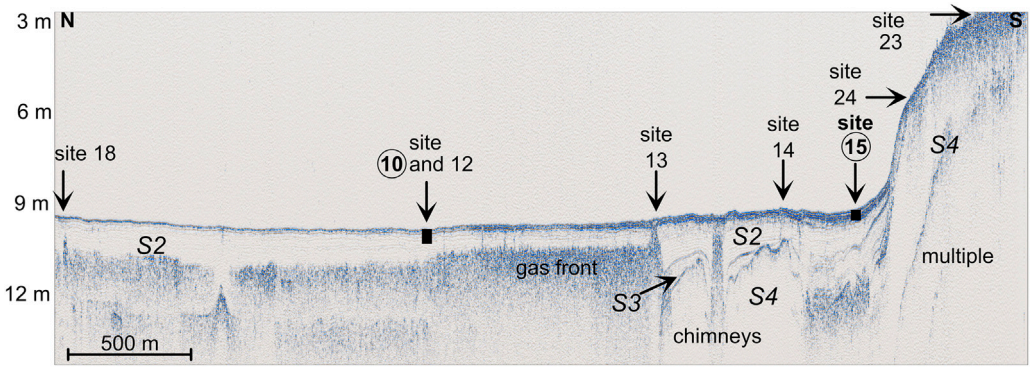

FIGURE 10 | Sediment acoustic profile of the western N-S transect in WB. The cores are represented as a circle around the site number, and the length of each core is indicated by the black bar.

(e.g., Böttcher et al., 2000; Al-Raei et al., 2009; Lipka et al., 2018b).

Except for sites 10 and 11 (**Figure 1**), pore water salinities in the WB sediments were characterized by relatively constant values (**Figures 6A**). Slight maxima around 10 to 15 cmbsf were observed at all sites and are due to past changes of bottom water salinities which are consequence of intrusion of salty North Sea water intrusions into the southern BS (Matthäus and Lass, 1995; Mohrholz, 2018).

Pore water salinities at Site 10 and in particular at Site 11 show a different pattern. Below the surface maxima, they decrease, and at Site 11 the values even reach fresh water conditions at the lowermost depth (salinity of about 1). It suggests that the sediments below the surface muds may host an aquifer containing fresh water, situated above glacial deposits and potentially part of seismic unit 3 (**Figure 11**). The pore water gradients of Site 11 (**Figure 6A-2**) result from mixing between endmembers (e.g., ground water and BS), superimposed by diagenetic reactions leading to further accumulation of some elements in the top sediments.

The pore waters at sites not impacted by freshening (sites 2, 15, 20, and 31) are characterized by a continuous increase in metabolite concentrations and a decrease in SO_4 and $\delta^{13}C_{DIC}$ values (**Figures 6J–O**). These vertical profiles are shaped by intense OM mineralization catalyzed by microorganisms using in particular SO_4 as terminal electron acceptors (Froelich et al., 1979; Jørgensen, 1982).

The maxima in Si, P, DIC, Mn, and Fe concentrations at Site 11 at around 10 cmbsf are in agreement with higher loads of top sediments in metabolizable organic matter leading to enhanced mineralization when compared to the other sites (**Figures 6K-2–M-2,O-2**). These observations also demonstrate that the fresh ground water is not substantially enriched in those substances. The pore water at Site 11 is depleted in SO_4 due to both, microbial sulphate reduction in the upper part of the sediment, but in particular due to the dilution with the underlying ground water that is free of SO_4.

The high dissolved Fe and Mn concentrations observed in the top sediments (**Figures 6L-2,M-2**) may accumulate due to the chemical reaction of metal ox (yhydrox)ides by biogenic sulphide

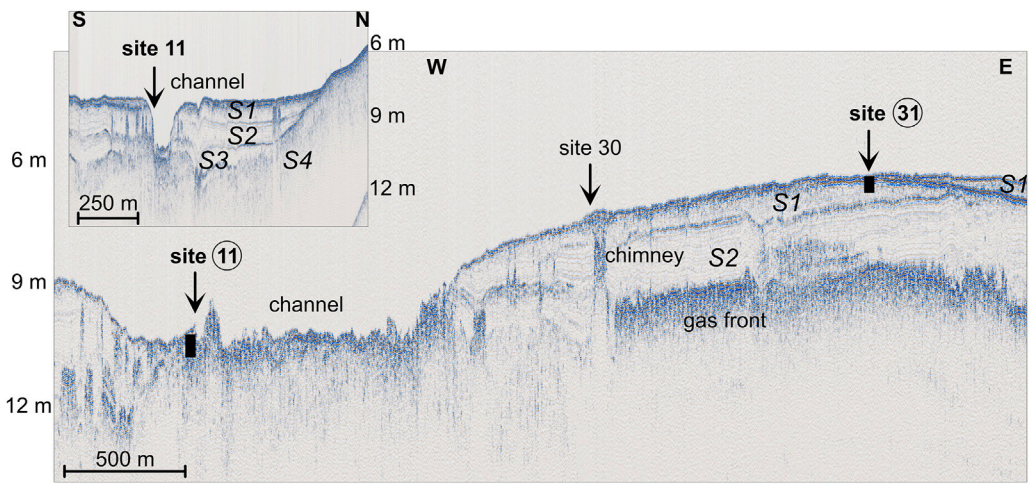

FIGURE 11 | Sediment acoustic profile of the eastern W-E transect. The cores are marked as a circle around the site number, and the length of each core is denoted by the black bar. Inset: perpendicular S-N transect highlighting site 11.

TABLE 3 | Summary of the terms used in the Ra mass balance.

Term	Definition	Value	±	Units	Source
A_{WB}	WB surface area–study area	81,472,500		m^2	Calculated from the bathymetry (GDI-BSH, 2020)
A_{WB}	assumed area where SGD take place	270,000		m^2	
V	WB volume - study area	430,812,610		m^3	Calculated from the bathymetry (GDI-BSH, 2020)
h	average depht of the bay	5		m	V/A_{WB}
Q_{str}	Discharge for the 3 western streams	1,515		$m^3\ d^{-1}$	Because there were no hydrologic data available for these streams, the value was taken from another stream close to area (LUNG, 2020)
Q_{str}	Discharge from Wallenstein stream	26,524		$m^3\ d^{-1}$	LUNG, (2021)
WA	Water age	5	1	d	(ln ($^{224}Ra/^{223}Ra$)WB–ln ($^{224}Ra/^{223}Ra$)beach pore water)/λ223 - λ223
Q_{out}	Water outflow	0.3		Bq d^{-1}	($^{224}Ra_{WB}$–$^{224}Ra_{offshore}$) *v/RT
C_{str}	$^{224}Ra_{ex}$ concentration in Wallenstein stream	5.8		Bq m^{-3}	this study–**Table 1**
C_{str}	$^{224}Ra_{ex}$ concentration in the western stream	1.1		Bq m^{-3}	this study–**Table 1**
C_{str}	$^{224}Ra_{ex}$ concentration in the western stream	2.6		Bq m^{-3}	this study–**Table 1**
C_{str}	$^{224}Ra_{ex}$ concentration in the western stream	4.1		Bq m^{-3}	this study–**Table 1**
$C_{offshore}$	$^{224}Ra_{ex}$ concentration in the open BS (Site 1)	0.2		Bq m^{-3}	this study
C	Average of ^{224}Ra inventory concentration in the WB	1.4	0.8	Bq m^{-3}	this study
λ	$^{224}Ra_{ex}$ decay constant	0.189		d^{-1}	
F_{sed}	Sediment diffusion from seabed	0.5	0.03	Bq $m^{-2}\ d^{-1}$	Krall et al. (2017)
F_{SGD}	$^{224}Ra_{ex}$ inputs from pore water fluxes	261.7		Bq $m^{-2}\ d^{-1}$	this study–**Table 1**
$C_{endmember}$	$^{224}Ra_{ex}$ of beach pore water (endmember)	51		Bq m^{-3}	this study–**Table 1**
$C_{endmember}$	$^{224}Ra_{ex}$ of beach pore water (endmember)	65		Bq m^{-3}	this study–**Table 1**
$C_{endmember}$	$^{224}Ra_{ex}$ of beach pore water (endmember)	84		Bq m^{-3}	this study–**Table 1**
$C_{endmember}$	$^{224}Ra_{ex}$ of beach pore water (endmember)	88		Bq m^{-3}	this study–**Table 1**
V_{SGD}	Volumetric SGD flow	3.8	0.7	cm d^{-1}	$F_{SGD}/C_{endmember}$

(e.g., Moeslund et al., 1994; Thamdrup et al., 1994; Böttcher et al., 2000). At the sediment-water interface, Fe and in part Mn may are oxidized by NO_3 and/or O_2, whereas in deeper sediment layers Fe and Mn may react with H_2S and DIC to form Fe sulphides and MnCa carbonate solid-solutions, respectively (Froelich et al., 1979; Berner, 1980; Huckriede and Meischner, 1996; Böttcher and Dietzel, 2010). The observed near-surface maximum in dissolved P at Site 11 is due to the parallel release from OM and reduction of Fe ox(yhydrox)ides that acted previously as sorption substrate for P (e.g., Haese, 2006).

The surface sediments at all sites are low in accumulating TS (considered to reflect essentially pyrite contents) when compared to the predicted Holocene saturation line (**Figure 8**), indicating the impact of sulphate-independent mineralization processes in the top sediments and the impact of bioturbation-driven-re-oxidation of sedimentary sulphur species (e.g., Jørgensen and Kasten, 2006). This is in line with previous observations (Mossmann et al., 1991; Böttcher et al., 2000) that gave evidence that for modern sediments some burial at depth and associated time is necessary to establish a constant TOC/S ratio. However, the freshening of pore water at Site 11 establishes SO_4 limited conditions and caused the TOC/TS ratio to remain below 2.8 (**Figure 8**).

Overall, the modeled mineralization rates at the WB are at the lower end when compared to measured gross sulphate reduction rates in muddy sediments from German coastal areas (Böttcher et al., 2000; Llobet-Brossa et al., 2002; Al-Raei et al., 2009; Lipka et al., 2018b) which is likely due to some H_2S reoxidation by metal oxy (hydrox)ides taken place in the surface sediments (Jørgensen, 1982). The highest net anaerobic mineralization rates are found at Site 11 (**Table 2**). The excavation of sediment (**Figure 11**) formed a local sediment trap and led to a fast accumulation of sediments as reflected by the homogeneous distribution of sedimentary organic matter, reactive metals like Fe and Mn, and anthropogenic tracers (Hg, Pb*) (**Figure 9**). This accumulation further leads to enhanced availability of fresh organic matter fostering microbial activity (Aller and Blair, 1996; Jørgensen and Kasten, 2006), and therefore, higher diagenetic element fluxes across the sediment-water interface (**Table 2**).

Moreover, the modeled fluxes indicate that advective and diffuse components are taking place, however, the last one has been more pronounced. DIC is liberated from deeper sediments to the bottom waters, especially at Site 11 (**Table 2**). The pore water at Site 11 was physicochemically evaluated by the Phreeq-C package (Parkhurst and Appelo, 1999). Assuming an equilibrium with

calcite at depth (Morse and Mackenzie, 1990) all solutions are characterized by an enhanced CO_2 partial pressure higher than atmospheric pressure. Therefore, the impact of fresh water at Site 11 on the bottom water of WB will enhance the capability of surface water to act as a potential CO_2 source for the atmosphere.

An Anthropogenic Bottle Opener for SGD?

A stronger decrease in salinity, and therefore an indication of fresh water occurrence is observed at Site 11 compared to the other sites (**Figure 6A-2**). The main morphological difference between this sites is the presence of an excavated navigation channel. This is an about 3–4 m deep artificial sedimentary depression (**Figure 11**) which was built for ship navigation channel between the open BS and the port of Wismar (VSW, 2018).

Based on the geophysical profiles, the dredging removed the previously overlying muddy sediments (units S1 and S2), thereby touching the underlying aquifer in unit 3 (**Figure 11**). The removal of the mud cover at Site 11 promotes the exchange of solutes and water between the aquifer and the bottom water. A more continued excavation this structure in the future, may enhance the direct impact of SGD on the WB. On the other hand, depending on the hydrographic boundary conditions, the artificial channel may also temporarily allow brackish water to penetrate the aquifer.

CONCLUSION AND OUTLOOK

The multi-tracer approach used in the present study demonstrated the impact of different fresh water sources on the Wismar Bay (WB), southern Baltic Sea, and in particular to prove the occurrence of SGD at the center of the bay. In addition, the change in the radium gradient towards the open sea suggests potential ground water leaking from the coastal borders in agreement with direct observations at the shoreline.

The sediment cores retrieved from the central part of the bay together with the acoustic survey discovered fresh water discharge at the sea bottom in the central part of the bay. The discovered SGD site (Site 11) is located in a navigation channel, which demonstrates that the dredging activity may have caused a change in the pressure gradient, thereby allowing ground water to penetrate the sediments overlying the aquifer and the bottom waters of the WB, respectively. Using a tentative Ra mass balance, we estimate a potential contribution from SGD to the WB of about 3.8 ± 0.7 cm d^{-1}.

Diagenesis in the surface sediments results in the enhancement of metabolites in the pore waters at depth. At Site 11, however, enhanced concentrations of metabolites were found in the top sediments which may also be related to the remineralization of fresh organic matter added by dredging in the past that lead to higher mineralization rates.

From the geochemical profiles it can be inferred that SGD is not just limited to the central part of, but can also occur in other places of the WB, which may or may not be associated with dredging activities. Therefore, explorations to determine the number of SGD sites are necessary.

Possible future engineering to impact the WB benthic structure may have impacts on benthic-pelagic coupling and, thereby, change the element fluxes into the bottom waters. Further studies, however, are required to investigate the potential impact of local sediment properties as a source for nutrients and dissolved carbon species for the WB water column.

DATA AVAILABILITY STATEMENT

The raw data supporting the conclusions of this article will be made available by the authors, and graphically presented data will be stored in the PANGEA data base.

AUTHOR CONTRIBUTIONS

MB, CVA, and JS developed the scientific concept and design of the study. CVA, JS, and PF, conducted the field campaigns and on-site measurements. IS, CVA, OD, SP, and PF carried out the analytical data measurements and processing. BL performed the reaction-transport modeling. CM and A-KJ contributed to the groundwater hydrogeochemistry and -geology and MZ was involved in data discussion. CVA and MB wrote the article with contributions and revisions from all co-authors. All authors agreed about the submission of the final version.

FUNDING

The study was supported by the German Academic Exchange Service (DAAD) via a PhD stipend for CvA to work in the Geochemistry & Isotope Biogeochemistry Group at IOW (project no. 57381412), and the Deutsche Forschungsgemeinschaft (DFG) to MB and A-KJ within the framework of the Research Training Group 'Baltic TRANSCOAST' funded by under grant number GRK 2000. This is Baltic TRANSCOAST publication no. GRK2000/0046. It is also supported by DFG to MB and JS within the KiSNet project. JS was further supported by the BONUS SEAMOUNT project funded jointly by the EU and the Federal Ministry of Education and Research of Germany (BMDF, grant no. 03F0771B) and by a FP7 EU Marie Curie Career Integration Grant (grant PCIG09-GA-2011-293499). MZ is supported by BMBF during DAM-MGF. BL acknowledges additional support from the Helmholtz Association (Alfred Wegener Institute Helmholtz Centre for Polar and Marine Research). We acknowledge financial support by Leibniz IOW for Open Access Publishing.

ACKNOWLEDGMENTS

The authors wish to thank the crew and captain of RV LITTORINA and M. Staniek for their expert technical on-board support, and S.

Plewe for his expert support during the field campaigns. We also wish to thank A. Köhler for expert ICP-OES support and I. Scherff for further laboratory assistance, B. Schnetger for providing a Th Standard, and J. Deepen (Stalu-MV) for providing the hydrological data. Aaron J. Beck and Olivier Radakovitch for the careful reviews that helped to improve the manuscript, and Henry Bokuniewicz for the editorial handling. MB further wishes to thank H.-J. H. Dohrenkamp, C.S. Henn, and The United Jazz + Rock ensemble for their culinary and musical inspirations during manuscript preparation. He dedicates this publication to the memory of T.G.P. Jones, C. Reiner, and U. Steinfurth, who recently passed away, for their inspiring and vital sense of humor.

SUPPLEMENTARY MATERIAL

The Supplementary Material for this article can be found online at: https://www.frontiersin.org/articles/10.3389/fenvs.2021.642346/full#supplementary-material

REFERENCES

Al-Raei, A. M., Bosselmann, K., Böttcher, M. E., Hespenheide, B., and Tauber, F. (2009). Seasonal Dynamics of Microbial Sulfate Reduction in Temperate Intertidal Surface Sediments: Controls by Temperature and Organic Matter. *Ocean Dyn.* 59, 351–370. doi:10.1007/s10236-009-0186-5

Aller, R. C., and Blair, N. E. (1996). Sulfur Diagenesis and Burial on the Amazon Shelf: Major Control by Physical Sedimentation Processes. *Geo-Marine Lett.* 16, 3–10. doi:10.1007/bf01218830

Beck, A. J., Tsukamoto, Y., Tovar-Sanchez, A., Huerta-Diaz, M., Bokuniewicz, H. J., and Sañudo-Wilhelmy, S. A. (2007). Importance of Geochemical Transformations in Determining Submarine Groundwater Discharge-Derived Trace Metal and Nutrient Fluxes. *Appl. Geochem.* 22, 477–490. doi:10.1016/j.apgeochem.2006.10.005

Bejannin, S., Tamborski, J. J., van Beek, P., Souhaut, M., Stieglitz, T., Radakovitch, O., et al. (2020). Nutrient Fluxes Associated with Submarine Groundwater Discharge from Karstic Coastal Aquifers (Côte Bleue, French Mediterranean Coastline). *Front. Environ. Sci.* 7, 205. doi:10.3389/fenvs.2019.00205

Berner, R. A. (1982). Burial of Organic Carbon and Pyrite Sulfur in the Modern Ocean; its Geochemical and Environmental Significance. *Am. J. Sci.* 282, 451–473. doi:10.2475/ajs.282.4.451

Berner, R. A. (1980). *Early Diagenesis: A Theoretical Approach*. Princeton, NJ: Princeton University Press.

Berner, R. A., and Raiswell, R. (1983). Burial of Organic Carbon and Pyrite Sulfur in Sediments over Phanerozoic Time: a New Theory. *Geochimica et Cosmochimica Acta* 47 (5), 855–862. doi:10.1016/0016-7037(83)90151-5

Blöschl, G., Bierkens, M. F. P., Chambel, A., Cudennec, C., Destouni, G., Fiori, A., et al. (2019). Twenty-three Unsolved Problems in Hydrology (UPH) – a Community Perspective. *J. Hydrol. Sci.* 64, 1141–1158.

Blott, S. J., and Pye, K. (2001). GRADISTAT: a Grain Size Distribution and Statistics Package for the Analysis of Unconsolidated Sediments. *Earth Surf. Process. Landforms* 26, 1237–1248. doi:10.1002/esp.261

Böttcher, M. E., and Dietzel, M. (2010). Metal-ion Partitioning during Low-Temperature Precipitation and Dissolution of Anhydrous Carbonates and Sulphates. *EMU Notes in Mineralogy* 10 (4), 139–187.

Böttcher, M. E., Hespenheide, B., Llobet-Brossa, E., Beardsley, C., Larsen, O., Schramm, A., et al. (2000). The Biogeochemistry, Stable Isotope Geochemistry, and Microbial Community Structure of a Temperate Intertidal Mudflat: an Integrated Study. *Continental Shelf Res.* 20, 1749–1769. doi:10.1016/s0278-4343(00)00046-7

Böttcher, M. E., Mallast, U., Massmann, G., Moosdorf, N., Mueller-Pethke, M., and Waska, H. (2021). "Coastal-Groundwater Interfaces (Submarine Groundwater Discharge)," in *Ecohydrological Interfaces*. Editors S. Krause, D. M. Hannah, and N. Grimm (New York, NY: Wiley & Sons).

Böttcher, M. E., and Schmiedinger, I. (2021). The Impact of Temperature on the Water Isotope ($^{2}H/^{1}H$, $^{17}O/^{16}O$, $^{18}O/^{16}O$) Fractionation upon Transport through a Low-Density Polyethylene Membrane. *Isotopes Environ. Health Stud.* 57, 183–192. doi:10.1080/10256016.2020.1845668

Boudreau, B. P., and Ruddick, B. R. (1991). On a Reactive Continuum Representation of Organic Matter Diagenesis. *Am. J. Sci.* 291, 507–538. doi:10.2475/ajs.291.5.507

Boudreau, B. P. (1997). *Diagenetic Models and Their Implementation: Modelling Transport and Reactions in Aquatic Sediments*. New York: Springer.

Brand, W. A., and Coplen, T. B. (2012). Stable Isotope Deltas: Tiny, yet Robust Signatures in Nature. *Isotopes Environ. Health Stud.* 48, 393–409. doi:10.1080/10256016.2012.666977

Burnett, W. C., Aggarwal, P. K., Aureli, A., Bokuniewicz, H., Cable, J. E., Charette, M. A., et al. (2006). Quantifying Submarine Groundwater Discharge in the Coastal Zone via Multiple Methods. *Sci. Total Environ.* 367, 498–543. doi:10.1016/j.scitotenv.2006.05.009

Burnett, W. C., Bokuniewicz, H., Huettel, M., Moore, W. S., and Taniguchi, M. (2003). Groundwater and Pore Water Inputs to the Coastal Zone. *Biogeochemistry* 66, 3–33. doi:10.1023/b:biog.0000006066.21240.53

Burnett, W. C., Peterson, R., Moore, W. S., and Oliveira, J. (2008). Radon and Radium Isotopes as Tracers of Submarine Groundwater Discharge – Results from the Ubatuba, Brazil SGD Assessment Intercomparison. *Est., Coast., Shelf Sci.* 76, 501–511. doi:10.1016/j.ecss.2007.07.027

Cerdà-Domènech, M., Rodellas, V., Folch, A., and Garcia-Orellana, J. (2017). Constraining the Temporal Variations of Ra Isotopes and Rn in the Groundwater End-Member: Implications for Derived SGD Estimates. *Sci. Total Environ.* 595, 849–857. doi:10.1016/j.scitotenv.2017.03.005

Church, T. M. (1996). An Underground Route for the Water Cycle. *Nature* 380, 579–580. doi:10.1038/380579a0

Clark, I., and Fritz, P. (1997). *Environmental Isotopes in Hydrogeology*. Boca Raton: Lewis Publishers, 138–140.

Claypool, G. E., and Kaplan, I. R. (1974). "The Origin and Distribution of Methane in Marine Sediments," in *Natural Gases in Marine Sediments*. Editor I. R. Kaplan (New York: Plenum Press), 99–140. doi:10.1007/978-1-4684-2757-8_8

Cline, J. D. (1969). Spectrophotometric Determination of Hydrogen Sulfide in Natural Waters. *Limnol. Oceanogr.* 14, 454–458. doi:10.4319/lo.1969.14.3.0454

de Souza, G. K., von Ahn, C. M. E., Niencheski, L. F. H., and de Andrade, C. F. F. (2021). Effects of Coastal Lagoon Water Level on Groundwater Fluxes of Nutrients to the Coastal Zone of Southern Brazil. *J. Mar. Sys.* 213, 103459. doi:10.1016/j.jmarsys.2020.103459

Dellwig, O., Wegwerth, A., Schnetger, B., Schulz, H., and Arz, H. W. (2019). Dissimilar Behaviors of the Geochemical Twins W and Mo in Hypoxic-Euxinic Marine Basins. *Earth-sci. Rev.* 193, 1–23. doi:10.1016/j.earscirev.2019.03.017

DWD (2020). Deutscher Wetterdienst 2019. Climate Data Germany – Wismar Station. Available at: https://cdc.dwd.de/portal/ (Accessed January 10, 2020).

Donis, D., Janssen, F., Liu, B., Wenzhöferö, F., Dellwig, O., Escher, P., et al. (2017). Biogeochemical Impact of Submarine Groundwater Discharge on Coastal Surface Sands of the Southern Baltic Sea. *Est., Coast., Shelf Sci.* 189, 131–142. doi:10.1016/j.ecss.2017.03.003

Douglas, A. R., Murgulet, D., and Peterson, R. N. (2020). Submarine Groundwater Discharge in an Anthropogenically Disturbed, Semiarid Estuary. *J. Hydrol.* 124369, 124369. doi:10.1016/j.jhydrol.2019.124369

Folk, R. L., and Ward, W. C. (1957). Brazos River Bar: a Study in the Significance of Grain Size Parameters. *J. Sed. Petrol.* 27, 3–26. doi:10.1306/74d70646-2b21-11d7-8648000102c1865d

Froelich, P. N., Klinkhammer, G. P., Bender, M. L., Luedtke, N. A., Heath, G. R., Cullen, D., et al. (1979). Early Oxidation of Organic Matter in Pelagic Sediments of the Eastern Equatorial Atlantic: Suboxic Diagenesis. *Geochim Cosmochim Acta* 43, 1075–1090. doi:10.1016/0016-7037(79)90095-4

Garcia-Solsona, E., Garcia-Orellana, J., Masqué, P., and Dulaiova, H. (2008). Uncertainties Associated with ^{223}Ra and ^{224}Ra Measurements in Water via a Delayed Coincidence Counter (RaDeCC). *Mar. Chem.* 109, 198–219. doi:10.1016/j.marchem.2007.11.006

Gat, J. (1996). Oxygen and Hydrogen Isotopes in the Hydrological Cycle. *Annu. Rev. Earth Planet. Sci.* 24, 225–262. doi:10.1146/annurev.earth.24.1.225

Gdi-Bsh (2020). GeoSeaPortal. Bundesamt fürfur Seeschiffahrt und Hydrographie. Available at: www.geoseaportal.de.

Gogina, M., Lipka, M., Woelfel, J., Liu, B., Morys, C., Böttcher, M. E., et al. (2018). In Search of a Field/based Relantioship between Benthic Macrofauna and Biogeochemistry in a Modern Brackish Coastal Sea. *Front. Mar. Sci.* 5, 489. doi:10.3389/fmars.2018.00489

Haese, R. R. (2006). in *The Biogeochemistry of Iron. Marine Geochemistry*. Editors H. D. Schulz and M. Zabel (Berlin: Springer-Verlag), 207–240.

Hennig, H., and Hilgert, T. (2007). Dränabflüsse – Der Schlüssel zur Wasserbilanzierung im nordostdeutschen Tiefland. – *Hydrologie und Wasserbewirtschaftung* 51 (6), 248–257.

Hilgert, T. (2009). Grundwasserneubildung Mecklenburg-Vorpommern-Aktualisierung und ergänzende Beschreibung, internal project report.

Hoefs, J. (2018). *Stable Isotope Geochemistry*. Springer-Nature, Science Ltd.

Huckriede, H., and Meischner, D. (1996). Origin and Environment of Manganese-Rich Sediments within Black-Shale Basins. *Geochimica et Cosmochimica Act* 8, 1399–1413. doi:10.1016/0016-7037(96)00008-7

Jankowska, H., Matciak, M., and Nowacki, J. (1994). Salinity Variations as an Effect of Groundwater Seepage through the Seabed (Puck Bay, Poland). *Oceanologia* 36, 33–46.

Jenner, A-K. (2018). Ground Water Development in North-Eastern Germany as Deduced from the Hydrogeochemical and Stable Isotopic Composition of Selected Drinking Waters. Griefswald: University of Greifswald and Leibniz IOW. [MSc thesis].

Johannes, R. E. (1980). The Ecological Significance of the Submarine Discharge of Groundwater. *Mar. Ecol. Prog. Ser.* 3, 365–373. doi:10.3354/meps003365

Jordan, H., and Weder, H. J. (1995). *Hydrogeologie – Grundlagen und Methoden und Regionale Hydrogeologie: Mecklenburg-Vorpommern, Brandenburg und Berlin, Sachsen-Anhalt, Sachsen, Thüringen*. Stuttgart: Enke Verlag, 603.

Jørgensen, B. B., and Kasten, S. (2006). in *Sulfur Cycling and Methane Oxidation. Marine Geochemistry*. Editors H. D. Schulz and M. Zabel (Springer), 271–309.

Jørgensen, B. B. (1982). Mineralization of Organic Matter in the Sea Bed: the Role of Sulphate Reduction. *Nature* 296, 643–645.

Jurasinski, G., Janssen, M., Voss, M., Böttcher, M. E., Brede, M., Burchard, H., et al. (2018). Understanding the Coastal Ecocline: Assessing Sea-Land-Interactions at Non-tidal, Low-Lying Coasts through Interdisciplinary Research. *Front. Mar. Sci.* 5 (342), 1–22. doi:10.3389/fmars.2018.00342

Kostka, J. E., and Luther, G. W. (1994). Partitioning and Speciation of Solid Phase Iron in Saltmarsh Sediments. *Geochim. Cosmochim. Acta* 58, 1701–1710. doi:10.1016/0016-7037(94)90531-2

Kotwicki, L., Grzelak, K., Czub, M., Dellwig, O., Gentz, T., Szymczycha, B., et al. (2014). Submarine Groundwater Discharge to the Baltic Coastal Zone: Impacts on the Meiofaunal Community. *J. Mar. Sys.* 129, 118–126. doi:10.1016/j.jmarsys.2013.06.009

Krall, L., Garcia-Orellana, J., Trezzi, G., and Rodellas, V. (2017). Submarine Groundwater Discharge at Forsmark, Gulf of Bothnia, provided by Ra Isotopes. *Mar. Chem.* 162, 162–172. doi:10.1016/j.marchem.2017.09.003

Lampe, R., Luebke, H., Endtmann, E., and Harff, J. (2013). A New Relative Sea-Level Curve for the Wismar Bay, N-German Baltic Coast. *Meyniana* 57, 5–35.

Lee, Y. W., Hwang, D-W., Kim, G., Lee, W-C., and Oh, H-T. (2009). Nutrient Inputs from Submarine Groundwater Discharge (SGD) in Masan Bay, an Embayment Surrounded by Heavily Industrialized Cities, Korea. *Sci. Tot. Env.* 407, 3181–3188. doi:10.1016/j.scitotenv.2008.04.013

Leipe, T., Moros, M., Kotilainen, A., Vallius, H., Kabel, K., Endler, M., et al. (2013). Mercury in Baltic Sea Sediments – Natural Background and Anthropogenic Impact. *Chem. der Erde* 73, 249–259. doi:10.1016/j.chemer.2013.06.005

Lipka, M., Böttcher, M. E., Wu, Z., Sültenfuß, J., Jenner, A-K., Westphal, J., et al. (2018a). Ferruginous Groundwaters as a Source of P, Fe, and DIC for Coastal Waters of the Southern Baltic Sea: (Isotope) Hydrobiogeochemistry and the Role of an Iron Curtain. *E3s Web Conf.* 54, 1–5. doi:10.1051/e3sconf/20185400019

Lipka, M., Woelfel, J., Gogina, M., Kallmeyer, J., Liu, B., Morys, C., et al. (2018b). Solute Reservoirs Reflects Variability of Early Diagenetic Processes in Temperate Brackish Surface Sediments. *Front. Mar. Sci.* 5, 413. doi:10.3389/fmars.2018.00413

Llobet-Brossa, E., Rabus, R., Böttcher, M. E., Könneke, M., Finke, N., Schramm, A., et al. (2002). Community Structure and Activity of Sulfate-Reducing Bacteria in an Intertidal Surface Sediment: A Multi-Method Approach. *Aquat. Microb. Ecol.* 29, 211–226. doi:10.3354/ame029211

Löffler, H., Adam, C. G. B., Brinschwitz, D., Gieseler, W., Ginzel, G., Grunske, K.-A., et al. (2010). Hydrochemische Typisierung für Grundwasser im Lockergesteinsbereich des norddeutschen Flachlandes. *Schriftenreihe für Geowissenschaften.* 18, 369–399. doi:10.1787/9789282102701-13-fr

Lung, M. V. (2009). Landesamt für Umwelt, Naturschutz und Geologie Mecklenburg-Vorpommern. Map of groundwater recharge, German: "Grundwasserneubildung", gwn.shp. Available at: https://www.umweltkarten.mv-regierung.de/script/ (Accessed December 14, 2019).

Lung, M. V. (2020). Landesamt für Umwelt, Naturschutz, und Geologie Mecklenburg-VorpommernKartenportal Umwelt Mecklenburg-Vorpommern. Data set "Grundwasserhöhengleichen". Available at: https://www.umweltkarten.mv-regierung.de/atlas/script/index.php (Accessed December 15, 2020).

Lung, M. V. (2021). Landesamt für Umwelt, Naturschutz, und Geologie Mecklenburg-Vorpommern. Lake Network Map of Mecklenburg Western-Pomerania: Gewässernetz M-V: Standgewässer: Seen, dlm25w_sg_seen.shp. Available at: https://www.umweltkarten.mv-regierung.de/atlas/script/index.php (Accessed December 14, 2020).

Macklin, P. A., Damien, T. M., and Santos, I. R. (2014). Estuarine Canal Estate Waters: Hotspots of CO_2 Outgassing Driven by Enhanced Groundwater Discharge? *Mar. Chem.* 167, 82–92. doi:10.1016/j.marchem.2014.08.002

Matthäus, W., and Lass, H. U. (1995). The Recent Salt Inflow into the Baltic Sea. *J. Phys. Oceanograph.* 25, 280–286. doi:10.1175/1520-0485(1995)025<0280:trsiit>2.0.co;2

Meister, P., Liu, B., Ferdelman, T. G., Jørgensen, B. B., and Khalili, A. (2013). Control of Sulphate and Methane Distributions in Marine Sediments by Organic Matter Reactivity. *Geochim. Cosmochim. Acta* 104, 183–193. doi:10.1016/j.gca.2012.11.011

Michaelis, J., Usdowski, E., and Menschel, G. (1985). Partitioning of ^{13}C and ^{12}C on the Degassing of CO_2 and the Precipitation of Calcite Rayleigh-type Fractionation and a Kinetic Model. *Am. J. Sci.* 285, 318–327. doi:10.2475/ajs.285.4.318

Moeslund, L., Thamdrup, B., and Jørgensen, B. B. (1994). Sulfur and Iron Cycling in a Coastal Sediment: Radiotracer Studies and Seasonal Dynamics. *Biogeochemistry* 27, 129–152. doi:10.1007/bf00002815

Mohrholz, V. (2018). Major Baltic Inflow Statistic – Revised. *Front. Mar. Sci.* 5, 384. doi:10.3389/fmars.2018.00384

Moore, W. S. (1996). Large Groundwater Inputs to Coastal Waters Revealed by ^{226}Ra Enrichments. *Nature* 380, 612–614. doi:10.1038/380612a0

Moore, W. S., and Arnold, R. (1996). Measurement of ^{223}Ra and ^{224}Ra in Coastal Waters Using a Delayed Coincidence Counter. *J. Geophys. Res.* 101, 1321–1329. doi:10.1029/95jc03139

Moore, W. S., and de Oliveira, J. (2008). Determination of Residence Time and Mixing Processes of the Ubatuba, Brazil, Inner Shelf Waters Using Natural Ra Isotopes. *Est.Coast. Shelf Sci.* 76, 512e521. doi:10.1016/j.ecss.2007.07.042

Moore, W. S. (2010). The Effect of Submarine Groundwater Discharge on the Ocean. *Annu. Rev. Mar. Sci.* 2, 59–88. doi:10.1146/annurev-marine-120308-081019

Moosdorf, N., Böttcher, M. E., Adyasari, D., Erkul, E., Gilfedder, B., Greskowiak, J., et al. (2021). A State-Of-The-Art Perspective on the Characterization of Subterranean Estuaries at the Regional Scale. *Front. Earth Sci.* 9, 601293.

Morse, J., and Mackenzie, F. T. (1990). *Geochemistry of Sedimentary Carbonates*. New York: Elsevier, 707.

Mossmann, J-R., Aplin, A. C., Curtis, C. D., and Coleman, M. L. (1991). Geochemistry of Inorganic and Organic sulphur in Organic-Rich Sediments from the Peru Margin. *Geochim. Cosmochim. Acta* 55, 3581. doi:10.1016/0016-7037(91)90057-c

Oberdorfer, J. A., Valentino, M. A., and Smith, S. V. V. (1990). Groundwater Contribution to the Nutrient Budget of Tomales Bay, California. *Biogeochemistry* 10, 199–216. doi:10.1007/bf00003144

Parkhurst, D., and Appelo, C. (1999). User's Guide to PHREEQC (Version 2): A Computer Program for Speciation, Batch-Reaction, One-Dimensional Transport, and Inverse Geochemical Calculations. *Water-Resources Invest. Rep.*, 99–4259. doi:10.3133/wri994259

Piper, A. (1944). A Graphic Procedure in the Geochemical Interpretation of Water Analyses. *Eos, Trans. Am. Geophys. Union* 25, 914–928. doi:10.1029/tr025i006p00914

Prena, J. (1995). Temporal Irregularities in the Macrobenthic Community and Deep-Water Advection in Wismar Bay (Western Baltic Sea). Estuarine. *Coastal Shelf Sci.* 41, 705–717. doi:10.1006/ecss.1995.0085

Rocha, C., Robinson, C. E., Waska, H., Holly, M. A., and Bokuniewicz, H. (2021). A Place for Subterranean Estuaries in Coastal Zone. Estuarine. *Coastal Shelf Sci.* 250, 107167. doi:10.1016/j.ecss.2021.107167

Rodellas, V., Garcia Orellana, J., Garcia-Solsona, E., Masque, P., Dominguez, J. A., Ballesteros, B. J., et al. (2012). Quantifying Groundwater Discharge from Different Sources into a Mediterranean Wetlandwetland by Using ^{222}Rn and Ra Isotopes. *J. Hydrol.* 466-467, 11–22. doi:10.1016/j.jhydrol.2012.07.005

Rodellas, V., Garcia-Orellana, J., Masqué, P., Feldman, M., and Weinstein, Y. (2015). Submarine Groundwater Discharge as a Major Source of Nutrients to the Mediterranean Sea. *PNAS March* 112 (13), 3926–3930. doi:10.1073/pnas.1419049112

Rodellas, V., Stieglitz, T. C., Tamborski, J. J., van Beek, P., Andrisoa, A., and Cook, P. G. (2021). Conceptual Uncertainties in Groundwater and Porewater Fluxes Estimated by Radon and Radium Mass Balances. *Limnol. Oceanogr.* 9999, 1–19. doi:10.1002/lno.11678

Santos, I. R., Chen, X., Lecher, A. L., Sawyer, A. H., Moosdorf, N., Rodellas, V., et al. (2021). Submarine Groundwater Discharge Impacts on Coastal Nutrient Biogeochemistry. *Nat. Rev. Earth Environ.* 2, 307–323. doi:10.1038/s43017-021-00152-0

Santos, I. R., Eyre, B. D., and Huettel, M. (2012). The Driving Forces of Porewater and Groundwater Flow in Permeable Coastal Sediments: A Review. *Estuarine, Coastal Shelf Sci.* 98, 1–15. doi:10.1016/j.ecss.2011.10.024

Santos, I. R., Niencheski, F., Burnett, W., Peterson, R., Chanton, J., Andrade, C. F. F., et al. (2008). Tracing Anthropogenically Driven Groundwater Discharge into a Coastal Lagoon from Southern Brazil. *J. Hydrol.* 353, 275–293. doi:10.1016/j.jhydrol.2008.02.010

Schafmeister, M-T., and Darsow, A. (2004). "Potential Change in Groundwater Discharge as Response to Varying Climatic Conditions – an Experimental Model Study at Catchment Scale," in *The Baltic Sea Basin*. Editors J. Harff and S. Bjorck (Springer), 449.

Schlitzer, R. (2001). Ocean Data View. Availableat: http://www.awi-bremerhaven.de/GEO/ODV.

Schlüter, M., Sauter, E., Andersen, C. E., Dahlgaard, H., and Dando, P. R. (2004). Spatial Distribution and Budget for Submarine Groundwater Discharge in Eckernförde Bay (Western Baltic Sea). *Limnol. Oceanogr.* 49 (1), 157–167. doi:10.4319/lo.2004.49.1.0157

Schultz, H. D. (2006). "Quantification of Early Diagenesis: Dissolved Constituents in Marine Pore Water," in *Mar. Geoch.* Editors H. D. Schulz and M. Zabel (Berlin, Heidelberg: Springer-Verlag).

Seeberg-Elverfelds, J., Schlüter, M., Feseker, T., and Kölling, M. (2005). Rhizon Sampling of Porewaters Near the Sediment-Water Interface of Aquitic Systems. *Limnol. Oceanogr.: Methods* 3, 361–371. doi:10.1002/lom3.v3.11

Smellie, J., Tullborg, E -L., Nilsson, A. C., Sandström, B., Waber, N., Gimeno, M., et al. (2008). *Explorative Analysis of Major Components and Isotopes—SDM-Site Forsmark*. SKB R- 08-84. Stockholm, Sweden: SKB.

Stegmann, S., Sultan, N., Kopf, A., Apprioual, R., and Pelleau, P. (2011). Hydrogeology and Ist Effect on Slope Stability along the Coastal Aquifer of Nice, France. *Mar. Geology* 280, 168–181. doi:10.1016/j.margeo.2010.12.009

Stieglitz, T. C., Rapaglia, J., and Kruoa, S. C. (2007). An Effect of Pier Pillings on Nearshore Submarine Groundwater Discharge from a (Partially) Confined Aquifer. *Estuaries and Coasts* 30 (3), 543–550. doi:10.1007/bf03036520

Stieglitz, T., Taniguchi, M., and Skyler, N. (2008). Spatial Variability of Submarine Groundwater Discharge. *Ubatuba, Brazil. Estuarine Coastal Shelf Science* 76, 493–500. doi:10.1016/j.ecss.2007.07.038

Szymczycha, B., Klostowska, Z., Lengier, M., and Dzierzbicka-Glowacka, L. (2020). Significance of Nutrients Fluxes via Submarine Groundwater Discharge in the Bay of Puck, Southern Baltic Sea. *Oceanologia* 62, 117–125. doi:10.1016/j.oceano.2019.12.004

Szymczycha, B., Vogler, S., and Pempkowiak, J. (2012). Nutrient Fluxes via Submarine Groundwater Discharge to the Bay of Puck, Southern Baltic Sea. *Sci. Total. Environ.* 438, 86–93. doi:10.1016/j.scitotenv.2012.08.058

Taniguchi, M., Dulaim, H., Burnett, K. M., Santos, I. R., Sugimoto, R., Stieglitz, T., et al. (2019). Submarine Groundwater Discharge Updates on its Measurement Techniques, Geophysical Drivers, Magnitudes, and Effects. *Front. Environ. Sci.* 7, 141. doi:10.3389/fenvs.2019.00141

Teatini, P., Isotton, G., Nardean, S., Ferronato, M., Mazzia, A., Da Lio, C., et al. (2017). Hydrogeological Effects of Dredging Navigable Channels Canals through Lagoon Shallows. A Case Study in Venice. *Hydrol. Earth Syst. Sci.* 21, 5627–5646. doi:10.5194/hess-21-5627-2017

Thamdrup, B., Fossing, H., and Jørgensen, B. B. (1994). Manganese, Iron, and Sulfur Cycling in a Coastal Marine Sediment, Aarhus Bay, Denmark. *Geochim. Cosmochim. Acta* 58, 5115–5129. doi:10.1016/0016-7037(94)90298-4

Virtasalo, J. J., Schroeder, J. F., Luoma, S., Majaniemi, J., Mursu, J., and Scholten, J. (2019). Submarine Groundwater Discharge Site in the First Salpausselkä Ice-Marginal Formation, South Finland. *Solid Earth-EGU* 10, 405–432. doi:10.5194/se-10-405-2019

VSW (2018). Wasserstrassen und Schiffahrtsverwaltung des Bundes. Anpassung der seewaertigen Zufahrt zum Seehafen Wismar. Availableat: https://www.gdws.wsv.bund.de/SharedDocs/Downloads/DE/Planfeststellungsverfahren/100_Anpassung_Wismar/Scopingunterlage.pdf?__blob=publicationFile&v=2 (Accessed July 10, 2020).

Whiticar, M. J., and Werner, F. (1981). Pockmarks: Submarine Vents of Natural Gas or Freshwater Seeps? *Geo-Marine Lett.* 1, 193–199. doi:10.1007/bf02462433

Winde, V., Böttcher, M. E., Escher, P., Böning, P., Beck, M., Liebezeit, G., et al. (2014). Tidal and Spatial Variations of DI^{13}C and Aquatic Chemistry in a Temperate Tidal basin during winter Time. *J. Mar. Syst.* 129, 394–402. doi:10.1016/j.jmarsys.2013.08.005

Conflict of Interest: The authors declare that the research was conducted in the absence of any commercial or financial relationships that could be construed as a potential conflict of interest.

The reviewer (AB) declared a past co-authorship with one of the authors (JS) to the handling Editor.

Publisher's Note: All claims expressed in this article are solely those of the authors and do not necessarily represent those of their affiliated organizations, or those of the publisher, the editors and the reviewers. Any product that may be evaluated in this article, or claim that may be made by its manufacturer, is not guaranteed or endorsed by the publisher.